ESD-TDR-65-306

Technical Report 385

Gunn Effect in Compound Semiconductors

A. G. Foyt, Jr.

7 July 1965

Prepared under Electronic Systems Division Contract AF 19(628)-5167 by

Lincoln Laboratory
MASSACHUSETTS INSTITUTE OF TECHNOLOGY
Lexington, Massachusetts

The work reported in this document was performed at Lincoln Laboratory, a center for research operated by Massachusetts Institute of Technology, with the support of the U.S. Air Force under Contract AF 19(628)-5167.

Distribution of this document is unlimited.

MASSACHUSETTS INSTITUTE OF TECHNOLOGY

LINCOLN LABORATORY

GUNN EFFECT IN COMPOUND SEMICONDUCTORS

A. G. FOYT, JR.

Group 85

TECHNICAL REPORT 385

7 JULY 1965

LEXINGTON MASSACHUSETTS

GUNN EFFECT IN COMPOUND SEMICONDUCTORS*

ABSTRACT

A theoretical and experimental study of the Gunn effect is presented. It appears that this effect, originally observed by Gunn as a time variation in the current through ohmic samples of n-GaAs when the sample voltage exceeded a critical value, can be accounted for by the transferred electron model of Ridley and Watkins. This model is based on a transfer of electrons from a low-mass, high-mobility conduction band that is lowest in energy to a higher-mass, low-mobility band as the electron temperature is increased by the applied electric field. If the transfer occurs rapidly enough as the electric field is increased, a bulk differential negative resistance will be realized, which then leads to the formation of domains of different electrical conductivity which move through the sample, giving rise to a time-varying current.

Most of the experimental results for n-GaAs verify this interpretation. The shape of the current vs time waveform, sharp spikes in current separated by flat valleys in current, for the longer samples ($\ell \sim 100$ to 1000 microns) and the observed independence of threshold electric field (2300 to 4000 volts/cm) on sample length are shown to be consistent with a negative resistance model. The value of electric field which characterized the regions of high conductivity, about 1500 volts/cm, is found to be independent of sample length as expected. In addition, the voltage across the high electric field domain is found to scale with sample length, also as expected, and the value of electric field which characterizes the regions of low conductivity is estimated to be $\geqslant$60,000 volts/cm. The effects of temperature on the threshold electric field and on the threshold electron drift velocity are consistent with the transferred electron model. For short samples ($\ell \sim 25$ to 100 microns), a sinusoidal current vs time waveform is seen, and for samples in the 100-micron length range, the sinusoidal mode is seen near threshold, and the spike mode is seen well above threshold. Although the sinusoidal mode is not predicted by the simplest form of the model, the effects of mognetic field and termination impedance on this mode are consistent with the interpretation of this mode as a longitudinal disturbance caused by a negative resistance.

The Gunn effect has also been observed in n-CdTe, and resistance vs hydrostatic pressure experiments show that the transferred electron model is a reasonable explanation for this material as well.

Finally, the absence of an instability in n-InSb and n-InAs is shown to be consistent with the transferred electron model. The higher conduction band minima in these materials are probably sufficiently separated from the lowest minimum that other effects, such as carrier multiplication, will occur before transfer, and no negative resistance is to be expected.

Accepted for the Air Force
Stanley J. Wisniewski
Lt Colonel, USAF
Chief, Lincoln Laboratory Office

---

*This report is based on a thesis of the same title submitted to the Department of Electrical Engineering at the Massachusetts Institute of Technology on 14 May 1965, in partial fulfillment of the requirements for the degree of Doctor of Science.

CONTENTS

GUNN EFFECT IN COMPOUND SEMICONDUCTORS

CHAPTER I
INTRODUCTION AND BACKGROUND

A. INTRODUCTION

The purpose of this report is to explore experimentally the current instability known as the Gunn effect and to examine a model for the phenomenon.

This effect, first observed by Gunn[1-3] in samples of n-type GaAs, is a time instability in the sample current when the sample voltage is increased beyond a threshold value. The instability occurs in n-type samples with ohmic contacts at, above, and below room temperature with no external magnetic field. It takes the form of a variation in the sample current with time when the sample is driven from a voltage source. On several samples, Gunn observed this variation as a repetitive waveform with period $\tau = \ell/v_d$, where ℓ is the sample length, and v_d is the drift velocity of the electrons at threshold.

B. PREVIOUS HIGH ELECTRIC FIELD WORK

The Gunn effect is surprising from many points of view. No corresponding instability had been seen in the rather extensive studies of high electric field effects in germanium and silicon. Instead, a smooth variation in the mobilities of n- and p-type germanium and silicon was seen by several authors.[4-7] In these materials the electron and hole mobilities remained constant for low electric fields, then began to decrease at moderate field strength (~ several hundred volts/cm) and finally became proportional to E^{-1} at high fields (several thousand volts/cm) so that the electron or hole velocity became independent of field (see Fig. 1).

Shockley[8] obtained qualitative agreement with this behavior by assuming that the electrons interacted with the lattice through acoustic scattering at low and moderate fields, and that the velocity saturation at high fields was due to the emission of optical phonons by the electrons. Using the same model, Conwell[9] achieved quantitative agreement for germanium by a more complete treatment of the electron-optical phonon interaction.

The experimental study of high electric field effects in compound semiconductors is much less complete than for silicon and germanium. Glicksman and Hicinbothem[10] (also Bok and Guthmann[11]) investigated high-field effects in InSb at 77°K and obtained quantitative agreement with a polar optical mode scattering model by Stratton[12] as shown in Fig. 2. It should be noted that the current never achieves a clear-cut saturation. Instead, the mobility decreases only slightly at moderate fields and then increases to values greater than its low-field value.

In contrast to the rather limited amount of experimental work, considerably more theoretical work has been done on the calculation of electric field effects in polar compounds.[13,14] Frohlich and Paranjape[15] studied the case in which the electron-electron interactions dominated

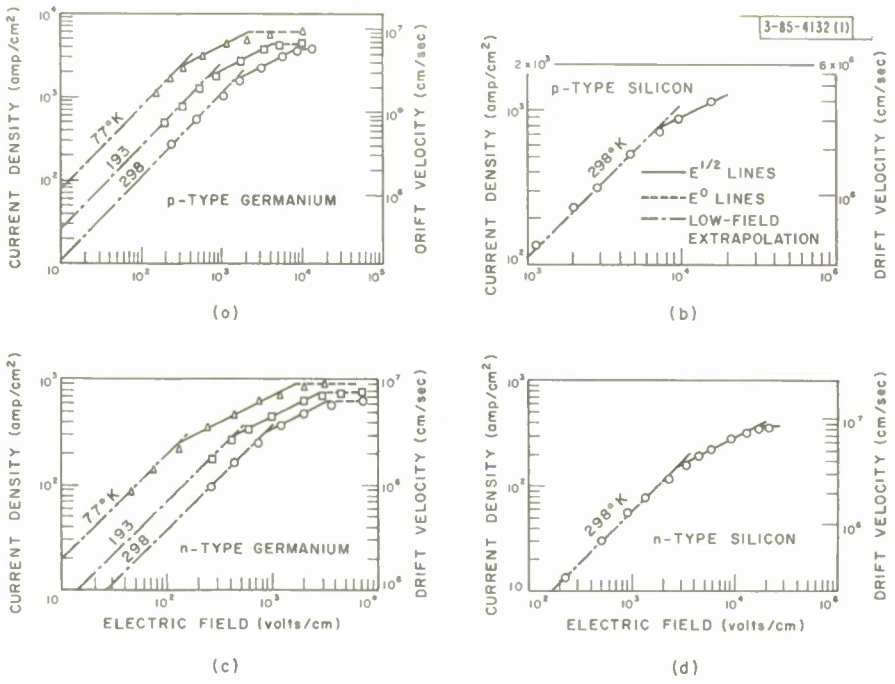

Fig. 1(a-d). Drift velocity vs electric field for germanium and silicon [after E. J. Ryder (Ref. 4)].

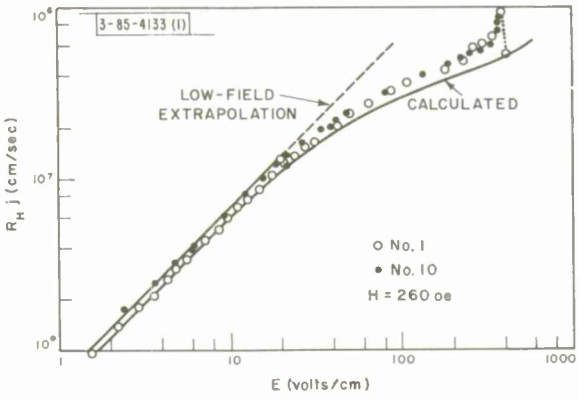

Fig. 2. Drift velocity vs electric field for InSb [after M. Glicksman and W. A. Hicinbothem, Jr. (Ref. 10)].

the electron motion so that the electron distribution was a shifted Maxwell-Boltzmann function of the form

$$f(\bar{p}) = a \exp\left[-\frac{(p - p_o)^2}{2mkT}\right]$$

where p_o and T are determined by the electron interaction with the electric field and the lattice. The work of Frohlich and Paranjape was directed toward dielectric breakdown phenomenon in polar crystals. Stratton[12] applied this approach to the calculation of mobilities in polar semiconductors from low fields up to breakdown. As mentioned earlier, this model was used successfully by Glicksman and Hicinbothem to explain their results for InSb. It will be seen later that a modified version of the model, which includes conduction in two bands, will explain the bulk of the high electric field behavior in the materials used in this study, although the low electric field behavior is, quite often, not explained.

Another approach to the calculation of low-field mobility must be used if electron-electron collisions are neglected. One such approach was used by Ehrenreich[16] to explain successfully the low-field mobility in n-type GaAs. This method is a variational technique[17,18] in which the solution of the Boltzmann equation is expressed as a ratio of determinants which may be evaluated to any degree of accuracy. The method has not, however, been extended to include the effects of large electric fields.

C. REVIEW OF WORK ON THE GUNN EFFECT

Since its discovery, the Gunn effect has stimulated a great deal of interest. As mentioned earlier, Gunn's original papers[1-3] identified many of the important experimental features of this effect. A further key experiment by Gunn[19] showed that the instability appears as a domain of high electric field moving through the sample from the negative contact to the positive contact. This experiment provided a valuable clue to the mechanism of the instability by showing that in the unstable region, the sample was divided into distinct regions of different electrical conductivity which moved through the sample at the electron drift velocity. Gunn then discussed the possible phenomenological origin of this domain motion in terms of a bulk differential negative resistance.

The application of this instability to the generation of microwave power has been investigated by several authors. Gunn[3] and also Hakki and Irvin[20] obtained power efficiencies approaching two percent with pulse operation, while Quist and Foyt[21] obtained efficiencies of over seven percent on the same basis. In addition, Hakki and Irvin[20] achieved efficiencies of two percent with CW operation. Braslau, et al.,[22] have also reported CW operation but with considerably less efficiency.

Several models have been proposed as explanations for the effect. Gunn originally discussed the possibilities of pinch effects, hot electron trapping, energy dependent scattering of electrons, transfer of electrons to secondary conduction band minima, two stream instabilities, acoustic wave amplification, and optical lattice wave amplification. He concluded that of these the most likely was amplification of optical lattice waves.

Kroemer[23] pointed out that the transfer of electrons to secondary conduction band minima was much more reasonable than Gunn had originally thought, since Hilsum[24] had in fact shown that it should be possible to transfer electrons to higher conduction band minima in GaAs with moderate electric fields (several thousand volts/cm) and that a differential negative resistance

could result from this transfer. In view of Ridley's[25] paper on domain formation as a consequence of such a bulk negative resistance, Kroemer concluded that the transfer of electrons to higher conduction band minima was probably the source of the Gunn effect.

Two recent experiments have provided strong support for the transferred electron model. Day[26] showed that in high resistivity GaAs, it was possible to ionize carriers from an impurity level about 0.4 ev below the conduction band by applying an electric field of about 5000 volts/cm. Since the only present explanation of the data is that the impurities are impact-ionized, the experiment seems to confirm Hilsum's suggestion that it is possible to give electrons enough energy to populate the secondary conduction band minima, which are about 0.36 ev above the lowest minimum, with electric fields of a few thousand volts/cm. In the second experiment, by Hutson, et al.,[27] it was shown that the threshold voltage required for the Gunn effect decreased with increasing hydrostatic pressure, with the threshold voltage decreasing from 220 volts at a pressure of 1 kilobar to about 150 volts at 25 kilobars for a sample 0.1 cm long. They concluded that since the only important material parameter which should be affected in this sample by hydrostatic pressure was the relative separation between conduction band minima, this experiment provided compelling evidence for the transferred electron model as the source of the Gunn effect. This model, which forms the basis of the theory of Chap. II, will be discussed in detail.

D. TRANSFERRED ELECTRON MODEL

The concept of transferring charge carriers between different regions in conduction or valence bands by means of an external electric field was proposed originally by Ridley and Watkins[28] who discussed the possibility of transferring charge carriers between two bands of different mobility in covalent semiconductors. This model deals with the details of the band structure of the material in question and the way in which the electrons interact with each other and with the lattice.

The type of band structure required is shown in Fig. 3. Two types of minima are required: a low-mass, high-mobility minimum that is lowest in energy; and higher minima with larger mass and smaller mobility. This model operates as follows. At low electric fields, most of the electrons are in the lowest minimum and the resistivity is low. As the electric field is increased, the average energy of the electrons is increased and some of them will transfer to the higher minima, thus raising the resistivity. If the transfer occurs rapidly as the electric field is increased, a differential negative resistance may be achieved. Ridley and Watkins[28] discussed the case of strained p-type germanium in which the degenerate valence bands are separated by external strain and in which the electrons interact with the lattice through the acoustic modes.

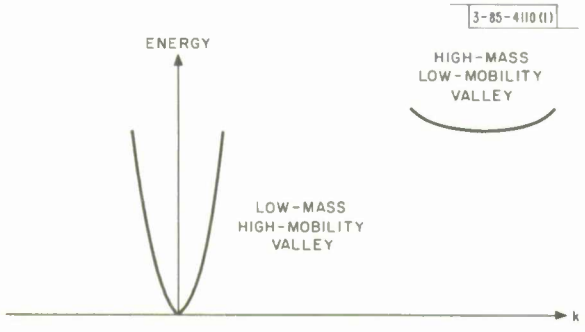

Fig. 3. Type of bond structure required for the transferred electron model.

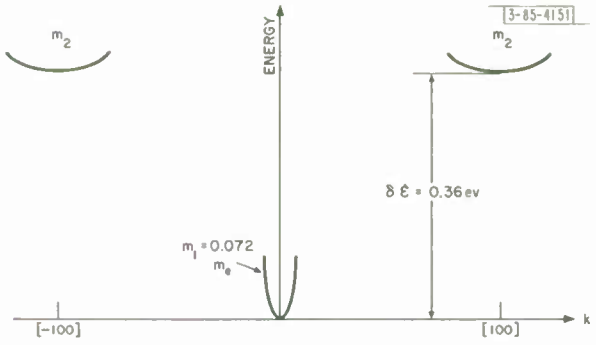

Fig. 4. GaAs conduction band structure.

Hilsum[24] modified this model for application to GaAs by using the band structure of Fig. 4 and assuming that the electrons interact with the lattice through the polar optical modes. In his calculation, Hilsum assumes that the electron-electron interaction is sufficiently strong so that the electron distribution can be described by a Maxwellian distribution function described in turn by an electron temperature T_e and a drift parameter p_o. He then calculates the current vs electric field relation using Stratton's[12] results, assuming that the electron-temperature and drift parameter are determined by the electron-lattice interaction for electrons in the lowest minimum, and that the upper levels are populated by being in thermal equilibrium with the lower minimum at the electron temperature. Hilsum then indicates that an appropriate generalization was made to include the effects of electron-lattice interaction in the second band. He includes the results of that calculation for one case in graphical form. The results of his calculation differ somewhat from those derived in Chap. II. The origin of this difference is not known at this time, but it presumably stems from different assumptions about the temperature and drift velocity in the second band.

E. SCOPE OF STUDY

Historically, this work progressed from an experimental investigation of the Gunn effect to the construction of a model. However, to achieve clarity of presentation, the model will be presented first. In Chap. II, the transferred electron model for polar materials will be presented. It will be shown that if the transfer of electrons occurs rapidly enough with increasing electric field, a bulk differential negative resistance will be realized. This model will then be applied in detail to three of the four materials used in the study: n-type GaAs, InSb, and InAs. It will be shown that GaAs should have a negative resistance region at room temperature, whereas InSb (at 77°K) and InAs probably would not. Following this will be a discussion of how a bulk differential negative resistance can lead to a time-varying current for a constant-voltage drive. The discussion of CdTe will be postponed to Chap. V because the parameters of the higher minimum are not known, and a calculation is not possible.

In Chap. III, the experimental techniques used to make the samples and to perform the electrical evaluation will be presented. Chap. IV will contain the experimental results, and Chap. V will be a discussion of the results and conclusions that can be made from this study.

CHAPTER II
THEORY AND CALCULATIONS

The first part of this chapter is devoted to a discussion of the transferred electron model as it applies to the materials used in this study and to a discussion of the assumptions which have been used in the calculation of electron drift velocity vs electric field relations. The details of the calculation are shown, and the model is then evaluated numerically for each of the materials under investigation. Finally, the relation between a bulk differential negative resistance and a time-varying current instability is discussed.

A. MODEL

The essential features of this model are the same as those for the model used by Hilsum which was discussed in Chap. I. We assume a band composed of two sets of minima: a low-mass, high-mobility minimum that is lowest in energy; and higher minima which have larger mass and smaller mobility as illustrated in Figs. 3 and 4. Also, we assume that the electron-lattice interaction is adequately described by interaction with the polar optical modes of the lattice. In order to proceed into the calculation of drift velocity vs electric field relations, we must now assume (or determine) the electron distribution function, that is, the way in which the electrons are distributed in energy within each valley and between different valleys. We assumed that the electrons within each valley could be characterized by a slightly displaced Maxwellian distribution function, and furthermore, that all the valleys shared a common temperature T_e so that the distribution function for the electrons in valley i would be of the form

$$f_i(\underline{p}) = a_i \exp\left[\frac{-(\underline{p}-\underline{p}_{oi}) \cdot \underline{\underline{m}}_i^{-1} \cdot (\underline{p}-\underline{p}_{oi})}{2kT_e}\right]$$

$$\approx a_i \left(1 + \frac{\underline{p}_{oi} \cdot \underline{\underline{m}}_i^{-1} \cdot \underline{p}}{kT_e}\right) \exp\left[\frac{-\underline{p} \cdot \underline{\underline{m}}_i^{-1} \cdot \underline{p}}{2kT_e}\right] \qquad (1)$$

where $\underline{\underline{m}}_i$ is the effective mass tensor of valley i. It was further assumed that the population in each of the subsidiary minima was the same and that the total population n_2 of the subsidiary minima would be related to the population n_1 of the lowest minimum by the Boltzmann factor

$$\frac{n_1}{n_2} = \frac{N_1}{N_2} e^{\delta\epsilon/kT_e} \quad . \qquad (2)$$

where N_1 is the density of states in the lowest minimum, N_2 is the total density of states in the higher minima, $\delta\epsilon$ is the energy separation between the lowest minimum and the higher minima, and $n_1 + n_2 = n$, the (constant) electron concentration. With this assumed distribution function, the Stratton model is easily generalized to include conduction in two bands.

This form of the electron distribution function was chosen because it allowed a simple explicit calculation of the drift velocity vs electric field relation and must be considered as, at best, a rough approximation to the actual situation. The electron densities in the samples that developed the Gunn effect were not sufficiently large to satisfy Stratton's criterion for the establishment of a Maxwellian distribution through electron-electron interactions. Also, in most

situations in which there are two kinds of particles, the heavier species will be characterized by a lower temperature than the lighter species, although both may be described by displaced Maxwellian distribution functions. In addition, all forms of scattering other than intravalley polar optical mode scattering are ignored.

In spite of all these difficulties, however, we shall see that our model explains many of the experimental results of this study.

B. CALCULATIONS

The rate of change of the distribution function for the electrons can be written as

$$\frac{\partial f}{\partial t} = \left(\frac{\partial f}{\partial t}\right)_e + \left(\frac{\partial f}{\partial t}\right)_E + \left(\frac{\partial f}{\partial t}\right)_L \tag{3}$$

where $(\partial f/\partial t)_e$, $(\partial f/\partial t)_E$, and $(\partial f/\partial t)_L$ are the rates of change due to electron-electron, electron-electric field, and electron-lattice interactions, respectively. In the steady state, $\partial f/\partial t = 0$. If Umklapp processes are neglected, crystal momentum and energy are conserved in electron-electron collisions so that

$$\int \underline{p} \left(\frac{\partial f}{\partial t}\right)_e d^3p = 0 \tag{4}$$

$$\int \epsilon_p \left(\frac{\partial f}{\partial t}\right)_e d^3p = 0 \tag{5}$$

where ϵ_p is the energy of a Bloch function of crystal momentum p. Hence, integrating (3) over momentum space, we obtain

$$\int \underline{p} \left(\frac{\partial f}{\partial t}\right)_L d^3p + \int \underline{p} \left(\frac{\partial f}{\partial t}\right)_E d^3p = 0 \tag{6}$$

$$\int \epsilon_p \left(\frac{\partial f}{\partial t}\right)_L d^3p + \int \epsilon_p \left(\frac{\partial f}{\partial t}\right)_E d^3p = 0 \quad . \tag{7}$$

For an applied electric field E in the z-direction,

$$\frac{dp_z}{dt} = -eE \quad ; \quad \frac{dp_y}{dt} = \frac{dp_x}{dt} = 0 \tag{8}$$

$$-\left(\frac{\partial f}{\partial t}\right)_E = -\frac{\partial f}{\partial p_z}\frac{dp_z}{dt} = eE\frac{\partial f}{\partial p_z} \quad . \tag{9}$$

Inserting (8) and (9) into (6) and (7), we obtain

$$eEn = \int p_z \left(\frac{\partial f}{\partial t}\right)_L d^3p \tag{10}$$

and

$$\underline{J} \cdot \underline{E} = \int \epsilon_p \left(\frac{\partial f}{\partial t}\right)_L d^3p \tag{11}$$

where $\underline{J}$ is the current density given by

$$\underline{J} = \int e\nabla_p \epsilon_p f(\underline{p})\, d^3p \tag{12}$$

and $\underline{J} \cdot \underline{E}$ is the input power density from the electric field.

Now, under the assumption that intravalley scattering controls the electron distribution, the electrons within each valley interact with the electric field independently so that the momentum and energy balance equations should be applied to each valley separately. However, to be consistent with our simplifying assumption of a common electron temperature, the energy balance equation must be applied only to the sum over all valleys. Consequently,

$$eEn_i = \int p_z \left(\frac{\partial f_i}{\partial t}\right)_L d^3p \tag{13}$$

and

$$\underline{J} \cdot \underline{E} = \sum_i \int \epsilon_p \left(\frac{\partial f_i}{\partial t}\right)_L d^3p \tag{14}$$

where f_i is assumed to be of the form given in (1). We will evaluate these terms separately for each valley: first for the lowest valley, which has spherical energy surfaces and a scalar effective mass, and then, by an appropriate generalization, for the higher valleys with ellipsoidal energy surfaces and tensor effective masses.

We may write $(\partial f_i/\partial t)_L$ in the form

$$-\left(\frac{\partial f_i}{\partial t}\right)_L = \sum_{\underline{q}} f_i(\underline{p})\, \rho_a(\underline{p}, \underline{p}+\underline{q}) - f_i(\underline{p}+\underline{q})\, \rho_e(\underline{p}+\underline{q}, \underline{p})$$

$$+ f_i(\underline{p})\, \rho_e(\underline{p}, \underline{p}-\underline{q}) - f_i(\underline{p}-\underline{q})\, \rho_a(\underline{p}-\underline{q}, \underline{p}) \tag{15}$$

where for polar optical mode interaction, the absorption and emission probabilities for a phonon of wavevector $\underline{q}$ are given by

$$\rho_a = \frac{2\pi}{\hbar} B(q)\, n_q\, \delta(\epsilon_F - \epsilon_I - k\Theta)$$

$$\rho_e = \frac{2\pi}{\hbar} B(q)\, (1 + n_q)\, \delta(\epsilon_F - \epsilon_I + k\Theta) \tag{16}$$

with

$k\Theta$ = optical phonon energy

$n_q = (\exp[\Theta/T_o] - 1)^{-1}$

ϵ_F = energy of final state of electron

ϵ_I = energy of initial state of electron

$$B(q) = \frac{e^2\hbar^2 k\Theta}{Vq^2}\left(\frac{1}{\epsilon_\infty} - \frac{1}{\epsilon_s}\right)$$

T_o = lattice temperature

ϵ_s = static dielectric constant

ϵ_∞ = high frequency dielectric constant.

Inserting (15) into (13) and (14), expanding the distribution functions to first order in the displacement p_o from equilibrium, and carrying out the integration over q, we obtain for valley 1,

$$eEn_1 = \frac{p_{01}}{3} \int p g_1(\underline{p})\, d^3p \tag{17}$$

$$\int \epsilon_p \left(\frac{\partial f_1}{\partial t}\right)_L d^3p = \frac{1}{2} \int \frac{p^2}{m_1} g_0(\underline{p})\, d^3p \tag{18}$$

where

$$g_0(\underline{p}) = \frac{eE_{01}N_o f_{10}(\underline{p})}{p} \left[\varphi_1(p^2)\left(1 - e^{\gamma_o - \gamma}\right)\right.$$

$$\left. + \varphi_1(p^2 - 2m_1k\Theta)\left(e^{\gamma_o} - e^{\gamma}\right)\right] \tag{19}$$

and

$$g_1(\underline{p}) = \frac{eE_{01}N_o f_{10}(\underline{p})}{m_1 kT_e} \left\{\varphi_1(p^2)\left[1 - \left(1 + \frac{m_1k\Theta}{p^2}\right)e^{\gamma_o - \gamma}\right]\right.$$

$$+ \varphi_1(p^2 - 2m_1k\Theta)\left[e^{\gamma_o} - \left(1 - \frac{m_1k\Theta}{p^2}\right)e^{\gamma}\right]$$

$$\left. + \frac{(p^2 + 2m_1k\Theta)^{1/2}}{p} e^{\gamma_o - \gamma} + \frac{(p^2 - 2m_1k\Theta)^{1/2}}{p} e^{\gamma}\right\} . \tag{20}$$

Here

$$\varphi_1(p^2) = \ln \frac{(p^2 + 2m_1k\Theta)^{1/2} + p}{(p^2 + 2m_1k\Theta)^{1/2} - p}$$

$$f_{10}(\underline{p}) = a_1 \exp\left[\frac{-p^2}{2m_1kT_e}\right]$$

$$eE_{01} = \left(\frac{1}{\epsilon_\infty} - \frac{1}{\epsilon_s}\right)\frac{m_1e^2k\Theta}{4\pi\hbar^2} \tag{21}$$

$$\gamma = \Theta/T_e$$

$$\gamma_o = \Theta/T_o$$

$$N_o = \frac{1}{e^{\gamma_o} - 1} .$$

Integration of (17) and (18) over p yields

$$E = G_1(\gamma)\, v_1 (m_1)^{3/2} \tag{22}$$

and

$$\int \epsilon_p \left(\frac{\partial f_1}{\partial t}\right)_L d^3p = G_2(\gamma)\, n_1 (m_1)^{1/2} \tag{23}$$

where $v_1 = p_{01}/m_1$ is the average drift velocity of valley 1,

$$G_1(\gamma) = \frac{eN_o}{6\pi\hbar^2} \left(\frac{k\Theta}{2\pi}\right)^{1/2} \left(\frac{1}{\epsilon_\infty} - \frac{1}{\epsilon_s}\right) \gamma^{3/2}\, e^{\gamma/2} \left[\left(e^{\gamma_o - \gamma} - 1\right) K_o\left(\frac{\gamma}{2}\right) + \left(e^{\gamma_o - \gamma} + 1\right) K_1\left(\frac{\gamma}{2}\right)\right] \tag{24}$$

and

$$G_2(\gamma) = \left(\frac{2}{\pi}\right)^{1/2} \frac{e^2 N_o (k\Theta)^{3/2}}{4\pi\hbar^2} \left(\frac{1}{\epsilon_\infty} - \frac{1}{\epsilon_s}\right) \gamma^{1/2}\, e^{\gamma/2} \left(e^{\gamma_o - \gamma} - 1\right) K_o\left(\frac{\gamma}{2}\right) \tag{25}$$

which are identical with Stratton's results. We note that the structure of the valley has entered these expressions only through the factors $(m_1)^{3/2}$ and $(m_1)^{1/2}$. We will now generalize this result for application to a set of subsidiary minima in a cubic material. Let us consider the case in which the external electric field is applied along a principal axis i of an ellipsoid and look first at the momentum transfer equation. It will contain terms on the right-hand side like

$$\int p_i \frac{p_i p_{oi}}{m_i} f_o(p)\, d^3p \int \frac{d^3q}{q^2}\, \delta(\epsilon_F - \epsilon_I \pm k\Theta) \tag{26}$$

where the subscripts i here denote the coordinate axis rather than the ellipsoid. If we now make the transformation

$$p_i = p_i' \sqrt{m_i} \tag{27}$$

which takes the ellipsoidal energy surfaces into spheres in the primed coordinate system, we obtain

$$p_{oi} \int p_i'^2\, f_o(p')\, d^3p' \int \frac{d^3q' \sqrt{m_1 m_2 m_3}}{\underline{q}' \cdot \underline{\underline{m}} \cdot \underline{q}'}\, \delta(\epsilon_F - \epsilon_I \pm k\Theta) \quad . \tag{28}$$

Ehrenreich[16] has shown that in the integration over q, it is an adequate approximation to replace the mass tensor by a scalar equal to the density of states mass $m_\rho = (m_1 m_2 m_3)^{1/3}$. By analyzing the other terms in the momentum loss equation in the same manner, we therefore find that

$$E \sim p_{oi} \sqrt{m_\rho} \sim v_i m_i \sqrt{m_\rho} \quad . \tag{29}$$

Since the high-field conductivity of a cubic material will remain isotropic under our approximations of equal electron temperature in all valleys and of first order expansion of the distribution function in the displacement p_{oi} from equilibrium, the orientation of the electric field may be taken in any convenient direction for purposes of calculation. For GaAs, which has a set of either three or six [100] subsidiary minima, it is particularly convenient to take the field in a [100] direction. Then (29) together with (22) leads to

$$\frac{E}{G_1(\gamma)} = v_{\ell 2} m_{\ell 2} \sqrt{m_{\rho 2}} = v_{t2} m_{t2} \sqrt{m_{\rho 2}} \tag{30}$$

where $m_{\ell 2}$ and m_{t2} are the longitudinal and transverse masses, respectively, of the subsidiary minima, $v_{\ell 2}$ is the drift velocity for the ellipsoids oriented along the field, v_{t2} is the drift velocity for those oriented transverse to the field, and $m_{\rho 2} = (m_{\ell 2} m_{t2}^2)^{1/3}$. In a similar manner, we examine the energy loss expression for the effects of anisotropy and find that

$$\int \epsilon_p \left(\frac{\partial f_o}{\partial t}\right)_L d^3p \tag{31}$$

$$\sim \int \underline{p} \cdot \underline{\underline{m}}^{-1} \cdot \underline{p} f_o(p)\, d^3p \int \frac{d^3q}{q^2}\, \delta(\epsilon_F - \epsilon_I \pm k\Theta) \tag{32}$$

$$\sim \int p'^2 f_o(p')\, d^3p' \int \frac{d^3q' \sqrt{m_1 m_2 m_3}}{\underline{q}' \cdot \underline{\underline{m}} \cdot \underline{q}'}\, \delta(\epsilon_F - \epsilon_I \pm k\Theta) \tag{33}$$

$$\sim \sqrt{m_\rho} \tag{34}$$

upon using the same approximations as in going from (28) to (29). For the six [100] minima, this result, together with (23), leads to

$$\sum_{\substack{[100] \\ \text{valleys}}} \int \epsilon_p \left(\frac{\partial f_i}{\partial t}\right)_L d^3p = G_2(\gamma)\, n_2 \sqrt{m_{\rho 2}} \quad . \tag{35}$$

Collecting (14), (22), (23), (31), and (35), we have

$$\frac{E}{G_1(\gamma)} = v_1 (m_1)^{3/2} = v_{\ell 2} m_{\ell 2} \sqrt{m_{\rho 2}} = v_{t2} m_{t2} \sqrt{m_{\rho 2}} \tag{36}$$

and

$$J \cdot E = G_2(\gamma)\, (n_1 \sqrt{m_1} + n_2 \sqrt{m_{\rho 2}}) \tag{37}$$

with

$$J = n_1 e v_1 + \frac{n_2 e (2 v_{t2} + v_{\ell 2})}{3} \quad . \tag{38}$$

Solving for E and $\bar{v} = J/ne$, we finally obtain

$$\frac{\bar{v}^2}{v_\Theta^2} = \frac{3}{\gamma} \frac{\left(e^{\gamma_o - \gamma} - 1\right) K_o(\frac{\gamma}{2})}{\left[\left(e^{\gamma_o - \gamma} - 1\right) K_o(\frac{\gamma}{2}) + \left(e^{\gamma_o - \gamma} + 1\right) K_1(\frac{\gamma}{2})\right]} \times \frac{\left(N_1 e^{\delta\epsilon/kT_e} + N_2 \sqrt{\frac{m_{\rho 2}}{m_1}}\right)\left(N_1 e^{\delta\epsilon/kT_e} + N_2 \frac{m_1^{3/2}}{m_{c2} \sqrt{m_{\rho 2}}}\right)}{\left(N_1 e^{\delta\epsilon/kT_e} + N_2\right)^2} \tag{39}$$

and

$$\frac{E^2}{E_{01}^2} = \frac{2}{3\pi} N_o^2 \gamma^2 e^{\gamma} \left(e^{\gamma_o - \gamma} - 1\right) K_o\left(\frac{\gamma}{2}\right)$$

$$\times \left[\left(e^{\gamma_o - \gamma} - 1\right) K_o\left(\frac{\gamma}{2}\right) + \left(e^{\gamma_o - \gamma} + 1\right) K_1\left(\frac{\gamma}{2}\right)\right]$$

$$\times \frac{\left(N_1 e^{\delta\epsilon/kT_e} + N_2 \sqrt{\frac{m_{\rho 2}}{m_1}}\right)}{\left(N_1 e^{\delta\epsilon/kT_e} + N_2 \frac{m_1^{3/2}}{m_{c2}\sqrt{m_{\rho 2}}}\right)} \qquad (40)$$

where

$$\frac{1}{m_{c2}} = \frac{1}{m_{\ell 2}} + \frac{2}{m_{t2}}$$

$$v_\Theta^2 = \frac{k\Theta}{m_1} \quad . \qquad (41)$$

These are parametric equations for $\bar{v}$ and E in terms of the electron temperature T_e. In order to find $\bar{v}$ vs E, these equations can be evaluated numerically,[29,30] for a given material, over a range of T_e.

C. APPLICATION OF THE MODEL

For n-GaAs, the following values[31] were used to evaluate the $\bar{v}$ vs E relation: $m_1 = 0.072\, m_e$, total density of states mass in the higher minima = $1.2\, m_e$ (Ref. 32), $k\Theta = 0.035$ ev, and $\delta\epsilon = 0.36$ ev. To obtain numerical values for $m_{\rho 2}$ and m_{c2}, we assumed that the anisotropy coefficient K is about 5, the same as for silicon, which gives $m_{\rho 2} = 0.36\, m_e$ and $m_{c2} = 0.29\, m_e$ for each of the six valleys. These values are used for the Case 1 curve shown in Fig. 5.

A difficulty with this case is that it underestimates the mobility ratio between the lowest minimim and the higher minima. This ratio was estimated by Ehrenreich as 50 or greater, and more recently by Hutson, et al.,[33] as 70 or somewhat less. If we take a value of 60 as a compromise estimate of mobility ratio, and assume that the decrease in mobility is entirely due to the larger mass of the higher valley, then as shown in Appendix A, we obtain $m_{\rho 2} = 1.2\, m_e$, $m_{c2} = 1.0\, m_e$, and a corresponding total density of states mass of $4.0\, m_e$. These values are used in Case 2 of Fig. 5. The values of density of states mass, the resulting ratio of density of states between the lowest minimim and the higher minima, $m_{\rho 2}$ and m_{c2} are summarized in Table I for the two cases. For n-CdTe, the parameters of the higher minima are not known. Some preliminary results from an experiment of resistance vs hydrostatic pressure, which will be discussed in Chap. IV, suggest that a set of minima of lower mobility than the lowest minimum is located a few tenths of an electron volt above the lowest minimum. The other parameters for n-CdTe, which will be used in Chap. V to discuss its low-field behavior, have been determined by Segall, Lorenz, and Halsted[34] as follows: $m_1 = 0.11\, m_e$, $k\Theta = 0.0213$ ev, $\epsilon_s = 10.6\, \epsilon_o$, $\epsilon_\infty = 7.13\, \epsilon_o$.

For n-type InSb and n-type InAs, the locations of the higher minima have not been determined. However, an extrapolation by Hilsum[35] of the energy gaps of the other III-V compounds

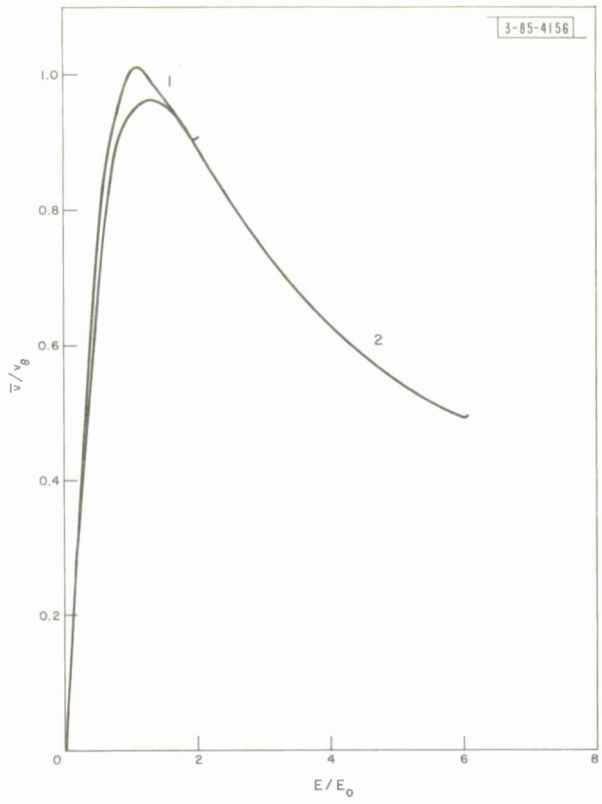

Fig. 5. Calculated drift velocity vs electric field for n-GaAs.

TABLE I
DENSITY OF STATES AND MASS RATIOS FOR GaAs

Case	Total Density of States Mass	N_2/N_1	$m_{\rho 2}$	m_{c2}	m_1
1	1.2 m_e	67	0.36 m_e	0.29 m_e	0.072 m_e
2	4 m_e	400	1.2 m_e	1.0 m_e	0.072 m_e

and of mixed crystals suggests that the next set of minima for each material is sufficiently far above the lowest minimum so that the higher minima would never be populated for the values of electron temperature up to breakdown. In this case, the model in the pre-avalanche region reduces to the one-band model of Stratton, for which the relation between the reduced electron drift velocity v/v_θ and the electric field E/E_o is completely determined by $\gamma_o = \theta/T_o$. This relation is given in Fig. 6 for several values of γ_o, where the curves appropriate for InSb at 77°K ($\gamma_o = 3.38$) and for InAs at 77°K ($\gamma_o = 4.42$) and 300°K ($\gamma_o = 1.13$) are identified. Table II gives the material parameters that determine v_θ and E_o for InSb and InAs.

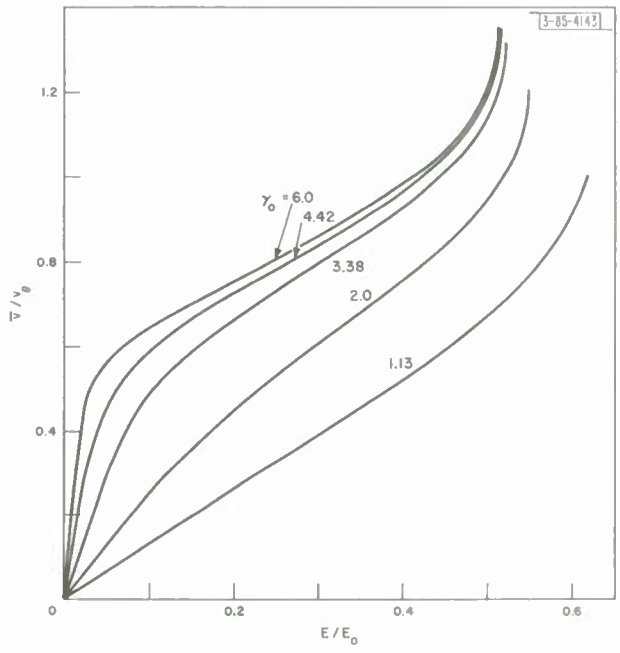

Fig. 6. Calculated drift velocity vs electric field for the one-band model.

TABLE II
PARAMETERS OF n-InAs AND n-InSb

Material	$k\theta$	m_1	ϵ_s	ϵ_∞	$\delta\epsilon$
InSb[31,36]	0.0225 ev	0.013 m_e	17.9 ϵ_o	15.7 ϵ_o	0.6 ev[35]
InAs[31]	0.0294 ev	0.02 m_e	14 ϵ_o	11.7 ϵ_o	1.0 ev[35]

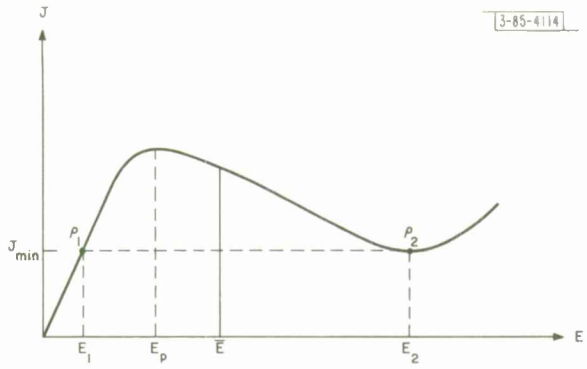

Fig. 7. Differential negative resistance, current vs electric field.

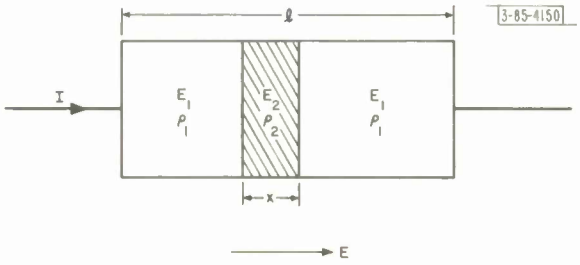

Fig. 8. Domain configuration.

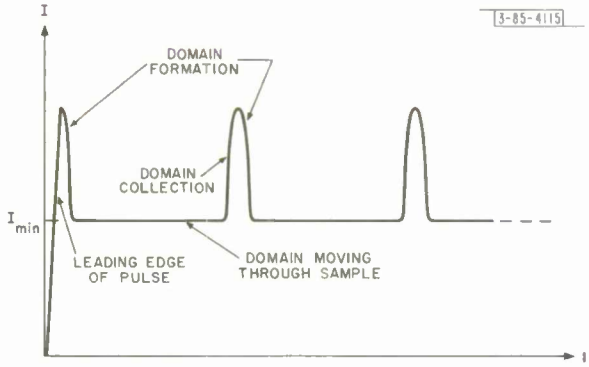

Fig. 9. Current vs time relation expected from a distributed differential negative resistance.

D. CONSEQUENCES OF A BULK DIFFERENTIAL NEGATIVE RESISTANCE

The negative resistance effect described in the previous section is of an essentially different character than most other voltage-controlled negative resistance effects (e.g., tunnel diodes) in that the effect is characteristic of a bulk of material rather than an interface. In contrast to the interface negative resistance, which can be stably biased in the negative resistance region, a bulk differential negative resistance can never be stably biased in the negative slope region. Instead, the bulk negative resistance becomes internally unstable when biased in this region.

Ridley[25] first treated the consequences of biasing a voltage-controlled bulk differential negative resistance from a voltage source. He used as a working hypothesis the assumption that the sample will take, if it can, a state of minimum entropy production. With this hypothesis, Ridley examined the behavior of a spontaneous perturbation in the resistivity in the material. He found that any such perturbation will decay if the slope of the current vs electric field is positive. On the other hand, for a negative slope, a perturbation which causes the current to decrease will grow. Ridley then interpreted this result as follows. In the former case, the sample will remain electrically uniform. In the latter case, a region of high electric field will form spontaneously somewhere in the sample, causing the sample current to decrease. This region of high electric field will continue to grow, causing the current to decrease until a minimum in the current vs electric field curve is reached. This domain of high electric field is still composed of electrons and will in general move under the influence of the external electric field. We therefore expect one of two situations to occur following the application of a voltage pulse. If the applied voltage biases the sample in an electric field less than E_p as seen in Fig. 7, then the sample current will follow the voltage pulse and remain at the value given by the current vs electric field curve. If, however, the applied electric field exceeds E_p, then the current will rise with the applied voltage to E_p. At that point, any spontaneous perturbation in the sample electron density that causes the sample current to decrease would grow in time and cause the sample current to decrease to its lowest value J_{min} consistent with the current vs electric field curve. This perturbed region would take the form of a region, or domain, of high electric field and high resistivity and would be characterized in the steady state by E_2, ρ_2, and J_{min}. The remainder of the sample would stay in the low resistance state characterized by E_1, ρ_1, and J_{min} so that a picture of the final configuration after the domain was completely formed would appear as in Fig. 8. This picture is, of course, for a steady state condition only, since the low- and high-field regions will move, in general, in the applied field. As the high-field region reaches a contact and is collected by that contact, the sample current will rise, and finally return to its threshold value. At this point, the cycle will repeat and will continue to repeat as long as the voltage is applied. The resulting current vs time waveform is shown in Fig. 9.

Several additional conditions must be met in order for this model to explain the Gunn effect. First, the domain of high electric field must be generated at a contact and travel the entire sample before it is collected. Second, the domain must travel at the drift velocity of the electrons. Third, the space charge regions necessary to terminate the high field in the domain must be small compared with the size of the domain. The first condition is necessary to explain the results of Gunn's probe measurement and the period vs transit time relation discussed in Chap. IV. It is not surprising that this situation should occur, since it is known that regions of metal-semiconductor alloy are disturbed regions in which a nonuniform electric field is very likely to occur. The velocity condition is necessary to explain the period vs transit time relation. As

Kroemer[37] has pointed out, this is reasonable in view of the size of E_2 ($\geq$60,000 volts/cm for GaAs as will be discussed later). Such a large value of E_2 requires a substantial amount of charge on both sides of the domain and results in a total depletion of mobile charge on the leading edge of the domain. This totally depleted layer should move at the drift velocity of the electrons. The third condition is met for the longer samples of GaAs as shown in Chap. IV.

There are several consequences of this model which will be compared with the experiments described in Chap. IV. The model predicts, for example, that the threshold electric field and, consequently, the electron drift velocity at threshold should be independent of the sample length. The model also predicts that the values of E_1, E_2, and the electron drift velocity at the current minimum v_{dv} should be independent of sample length. The model predicts a linear dependence on the high-field domain voltage with sample length as shown in the following derivation due to Ridley.

The applied voltage V_a must equal the voltages across the high- and low-field regions if the transition regions are neglected. Thus

$$V_a = E_2 x + E_1(\ell - x) = \bar{E}\ell \tag{42}$$

where $\bar{E} = V_a/\ell$ is the average electric field in the sample. This equation may be solved for x, the domain length, and we find

$$\frac{x}{\ell} = \frac{\bar{E} - E_1}{E_2 - E_1} \quad . \tag{43}$$

For GaAs, E_2 is much greater than E_1, as we shall see in Chap. IV, so that

$$\frac{x}{\ell} \approx \frac{\bar{E} - E_1}{E_2} \quad . \tag{44}$$

This relation may be solved for the domain voltage $E_2 x$ which is

$$E_2 x = (\bar{E} - E_1)\ell = V_a - E_1\ell \quad . \tag{45}$$

This relation will be examined in Chap. IV for GaAs.

If it is assumed that the current rise in the unstable region is entirely due to the uniform motion of a domain out of one contact, then we can establish a relation between the rise time of the current spike and the domain size as follows. The rise time of the current spike Δt corresponds to the uniform motion of a domain moving through the contact at the electron drift velocity v_{dv} so that this rise time is related to the domain length x by

$$x = v_{dv}\Delta t \quad .$$

This assumed relation will be used in Chap. IV to estimate the domain length for the longest GaAs samples.

CHAPTER III
EXPERIMENTAL TECHNIQUES

A. SAMPLE PREPARATION

All the samples used in this study were n-type compound semiconductors with free electron concentrations of 10^{14} to 10^{17}/cc at room temperature (77°K for InSb). The samples were made as small as possible to avoid Joule heating, since the power dissipated in even a small sample was large. Typical dimensions for the GaAs samples ranged from 150 × 150 microns in cross section for a 30-micron-long sample to 200 × 200 microns for a 1000-micron-long sample. In order to make samples of these dimensions with a uniform cross section, the following procedure was used for all the materials.

(1) Slices of 100 orientation were cut from a crystal.

(2) Standard lapping and etching techniques were used to reduce the slice thickness to 150 to 200 microns (for the longer samples) or to the desired sample length (for the shorter samples).

(3) The remaining four sides were cleaved so that the resulting sample was a rectangular parallelepiped.

Alloyed contacts to these samples were then made by placing the sample on a carbon heater strip hot stage in contact with the material to be alloyed to the sample. The sample (and alloy material) was then heated in a hydrogen and HCl atmosphere for a few seconds to perform the alloying operation. Figure 10 shows typical samples.

As a preliminary check on the quality of a sample, the low-field resistance was measured after the alloying operation. If the sample was ohmic and if it had about the correct resistance, as calculated from the bulk properties of the material, the sample was mounted in a tunnel diode package, as shown in Fig. 11, for further tests. A summary of the low-field electrical properties of the crystals used in the study is given in Table III. The details of etching, the types of contacts used, and the temperature of the alloy used for each material are given in Appendix B.

B. ELECTRICAL EVALUATION

In order to measure the I-V characteristics of these samples, some form of pulsed operation is needed to avoid sample heating. For some of the longest GaAs samples and for all the InAs samples, it was necessary to use very short pulses (~10 to 20 nsec) to avoid this problem. Pulsed operation was useful from another standpoint: it permitted examination of the starting transient of the instability. In order to achieve the requirements of a fast-rise pulse with a flat top, a pulse generator which discharged a coaxial delay line through a mercury-wetted relay was chosen. The fixture in which the sample is mounted must also be capable of high speed performance. Also, since it was clear from Gunn's original work that the instability could have components of high frequency, the fixture should be able to respond to those frequencies. Finally, it was decided to evaluate the samples in a resistive circuit in order to avoid obscuring the instability waveform with resonant structure circuits. The final evaluation circuit is shown in Fig. 12. The use of the 5-ohm resistor to terminate the pulse generator allows the same fixture to be used for a wide range of samples and permits evaluation of samples under voltage source conditions independent of changes in the sample impedance.

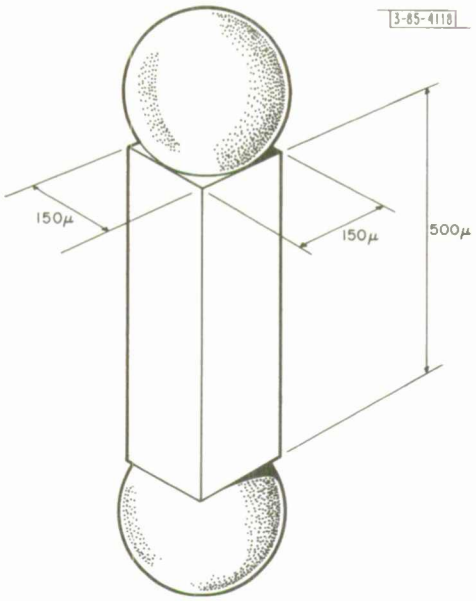

Fig. 10. Sketch of typical sample.

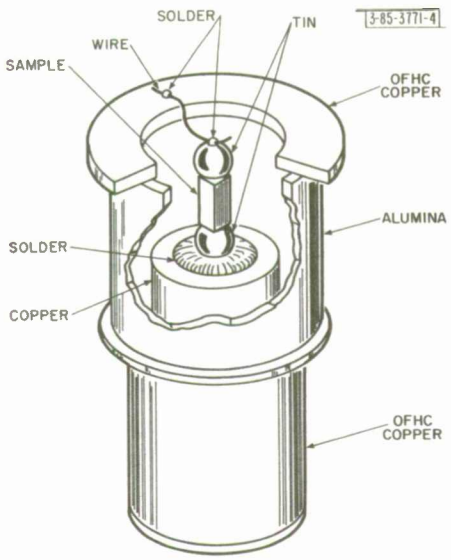

Fig. 11. Sketch af somple mounted in o package.

TABLE III
ELECTRICAL PROPERTIES OF CRYSTALS

Moterial	Crystal Na.	Temperature (°K)	Mobility (cm^2/valt-sec)	Carrier Concentration (carriers/cc)
n-GaAs	V254	300	5,200	3.6×10^{15}
n-GaAs	V254	77	9,300	2.4×10^{15}
n-GaAs	G161	300	5,360	$1.7 - 2.9 \times 10^{14}$
n-GaAs	G219	300	5,400	1.6×10^{15}
		77	9,370	5.2×10^{14}
n-CdTe	—	300	1,100	5×10^{14}
n-InSb	62-4	77	600,000	2.2×10^{14}
n-InAs	BU-1	300	25,500	2.4×10^{16}
n-InAs	BU-1	77	48,600	2.2×10^{16}

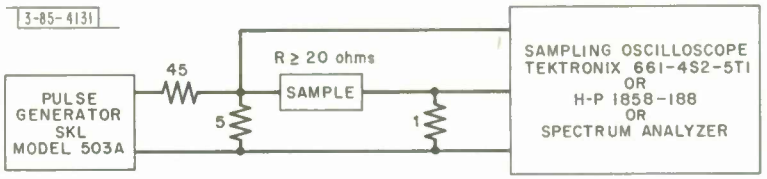

Fig. 12. Diagram of circuit used to measure sample current and voltage vs time.

The final sample holder, shown in Figs. 13 and 14, was designed to minimize lead inductance in all leads, to minimize feed-through capacity from the pulse generator to the current measuring resistor, and hopefully to allow the detection of waveforms containing frequencies of several gigacycles.

In order to evaluate the fixture, its pulse response was measured with a sample in place but with the pulse voltage below that required for instability. The pulse response of the current and voltage sampling probes on the fixture are shown in Figs. 15 and 16 and are to be compared with the pulse from the pulse generator.

Another measure of the response of the fixture is transmission loss as a function of frequency. The sine wave transmission loss, from input to the current sampling probe, was measured with a sample in place but with no external bias. The measured transmission loss is shown vs frequency in Fig. 17.

These measurements indicate that the fixture and associated equipment should be capable of detecting signals of at least 6 Gcps. This is not necessarily the case, however, because these measurements were made with a passive sample. Since we did not know of a method that would allow evaluation of the fixture when the sample was active, the response under these conditions is not known. However, signals as high as 4 Gcps have been seen from samples in the active region, and the frequency response of the fixture should not be changed very much, if at all, when the sample becomes active.

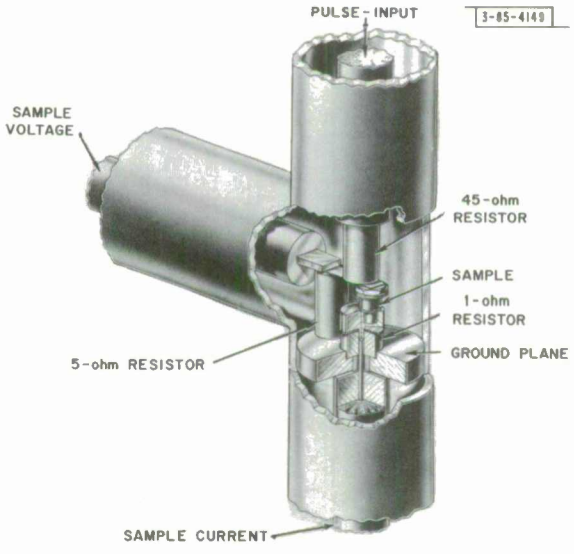

Fig. 13. Sample holder, perspective view.

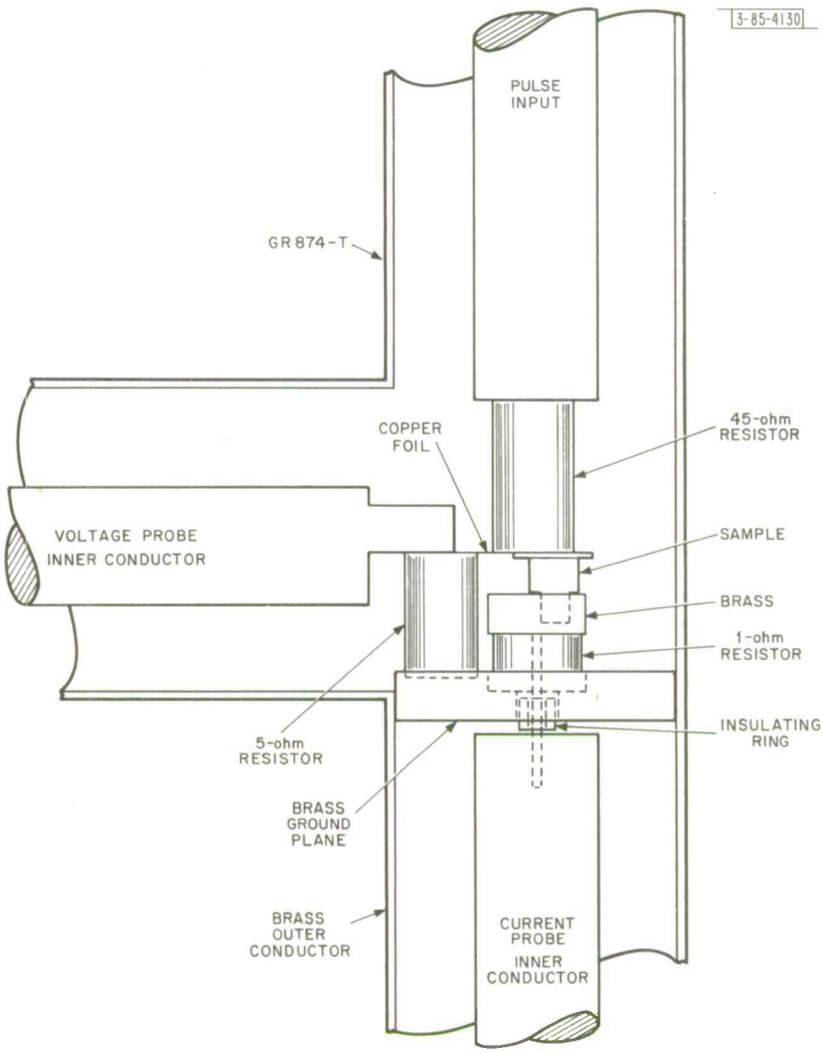

Fig. 14. Sample holder, scale drawing.

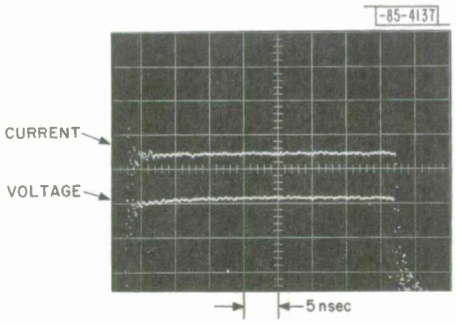

Fig. 15. Pulse response of sample holder.

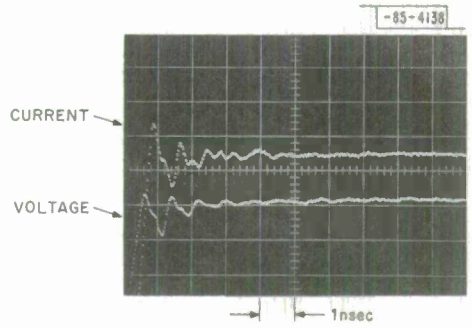

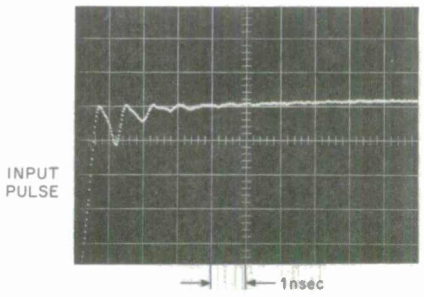

Fig. 16. Rise time of sample holder compared to rise time of input pulse.

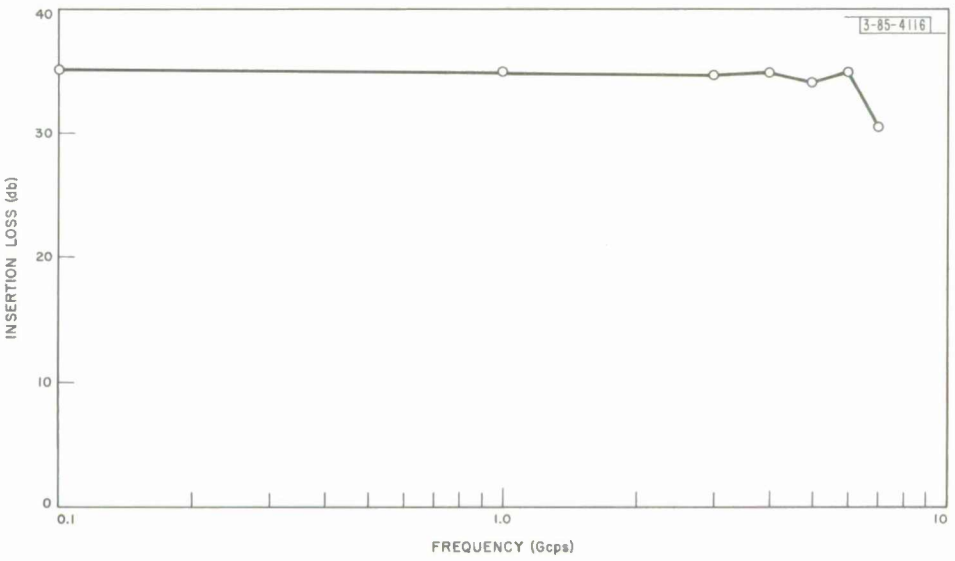

Fig. 17. Tronsmission loss vs frequency of sample holder.

CHAPTER IV
EXPERIMENTAL RESULTS

GaAs, which exhibited the strongest instability and which was readily obtained, was more intensively studied than the other materials. CdTe also displayed the instability but was less extensively studied. InSb and InAs, two materials which did not display the instability, were also examined.

A. GaAs

All the GaAs samples were prepared and evaluated as described in Chap. III. The voltage vs current characteristics for some typical samples are presented in Fig. 18. As shown, the current increases linearly with voltage (constant mobility) at low fields. As the voltage is increased further, the current increases more slowly (mobility decreasing) up to the instability threshold. Above threshold, the current varies in time for a constant voltage, and the average value of the current drops. The current in the unstable range varies from the threshold value (or slightly above that value) to lower values, as low as one-half the threshold value. This general character is true for all sample lengths that have been examined. However, there is a slight trend for the shorter samples to show more curvature before becoming unstable. The room temperature values of threshold electric field and threshold electron drift velocity are given in Figs. 19 and 20.

A change in the lattice temperature did not have an appreciable effect on the instability. However, there are slight trends in threshold electric field and peak electron drift velocity v_{dp}. The data for a few samples are compared to E_p and the peak calculated drift velocity v_p from Chap. II and are given in Figs. 21 and 22. As shown, there is no dramatic effect on the instability threshold with temperature. However, the direction of change of peak drift velocity is opposite to that expected from most plasma effects; i.e., in these effects, there is usually a competition between drift velocity and thermal velocity so that an increase in the lattice temperature would cause an increase in the threshold drift velocity.

In the unstable condition, the current may be seen on the sampling oscilloscope as a repetitive waveform for most samples. The shape of the current waveform in time varies a great deal from sample to sample. Also, the shape of the current waveform may depend on the driving voltage for a given sample. There are two characteristic waveforms that have been seen: sine waves and sharp spikes. Other types of waveforms occur but not in any consistent or repetitive manner. These various waveforms will be discussed in the next two sections.

1. Spike Waveforms

At voltages well above threshold (ten percent or more), up to several times the threshold voltage on the 100- to 1000-micron samples, the instability took the form of sharp spikes in the current vs time curve separated by longer intervals of smaller current, as indicated in Fig. 23 with the voltage waveforms shown for comparison. For these samples, the period vs transit time relation $\tau = \ell/v_{dv}$ was usually accurately obeyed, where v_{dv} is the electron drift velocity corresponding to the current minimum. The values of τ are given in Table IV (also Fig. 24) for several samples and compared to the observed period. These waveforms are initiated by the leading edge of the pulse. That is, the sample current rises with the sample voltage on the leading edge of the voltage pulse. As the voltage passes the threshold value, the

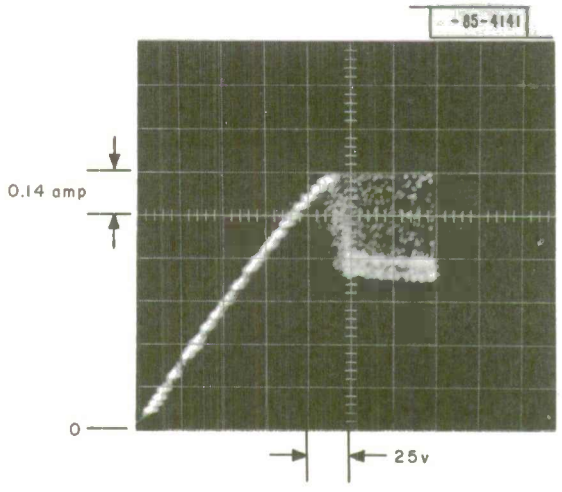

(a) Sample L15, ℓ = 327 microns.

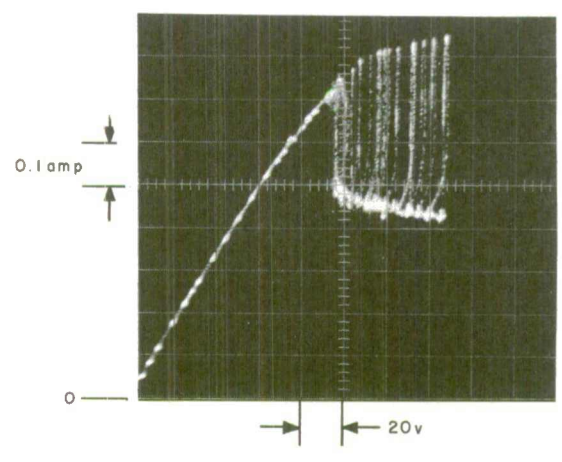

(b) Sample L2, ℓ = 272 microns.

Fig. 18 (a-d). Sample current vs voltage, GaAs, T = 300°K.

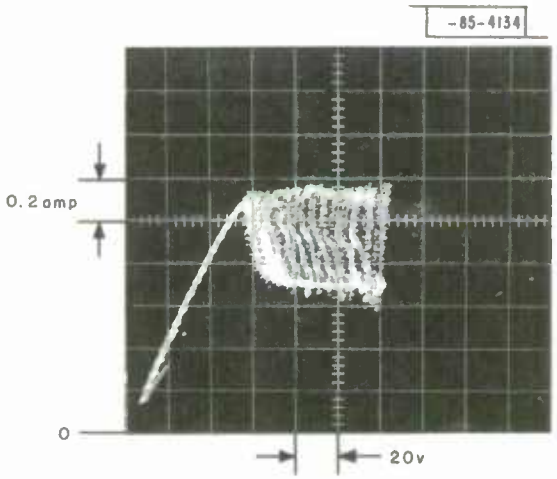

(c) Sample K40, ℓ = 172 microns.

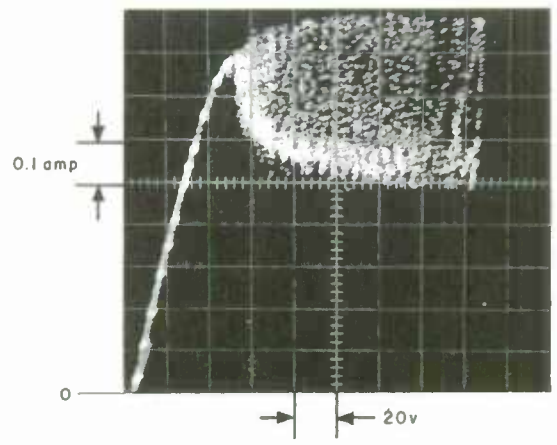

(d) Sample L29, ℓ = 127 microns.

Fig. 18. Continued.

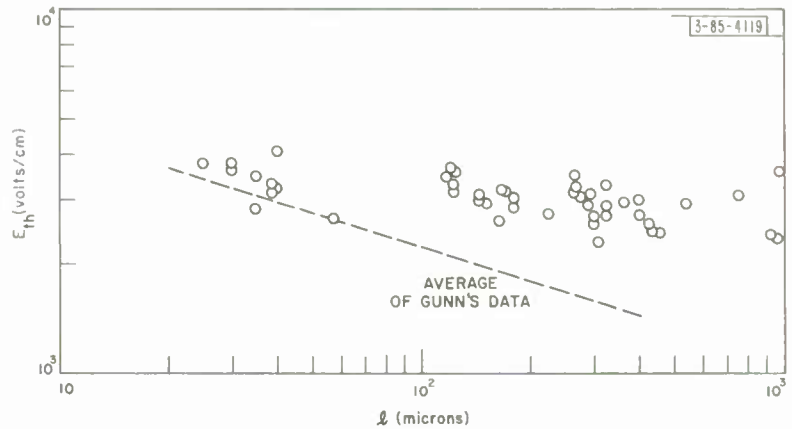

Fig. 19. Threshold electric field vs sample length, T = 300°K.

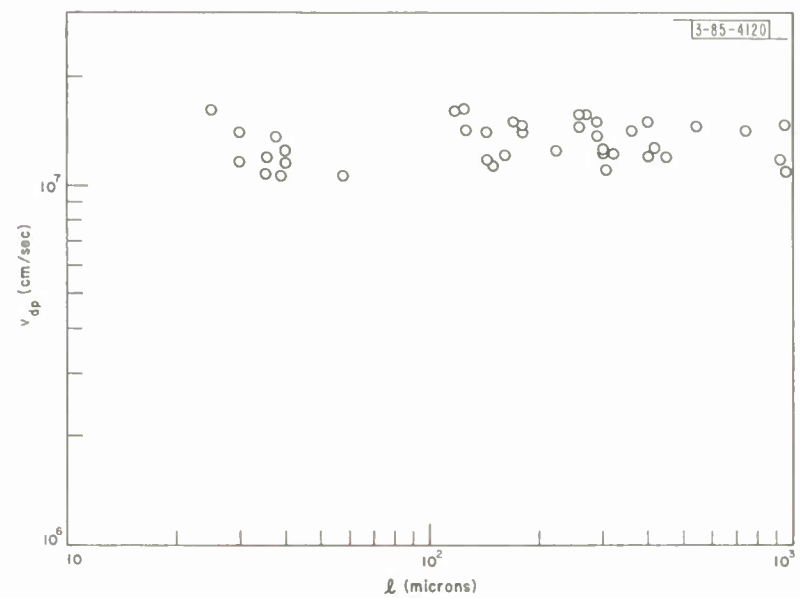

Fig. 20. Threshold electron drift velocity vs sample length, GaAs, T = 300°K.

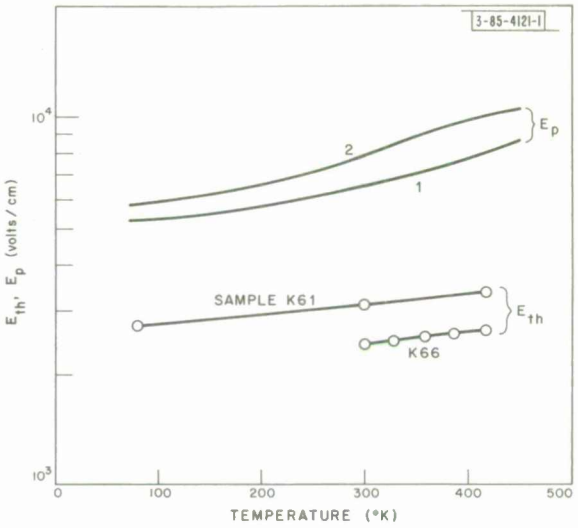

Fig. 21. Threshold electric field vs temperature, GoAs.

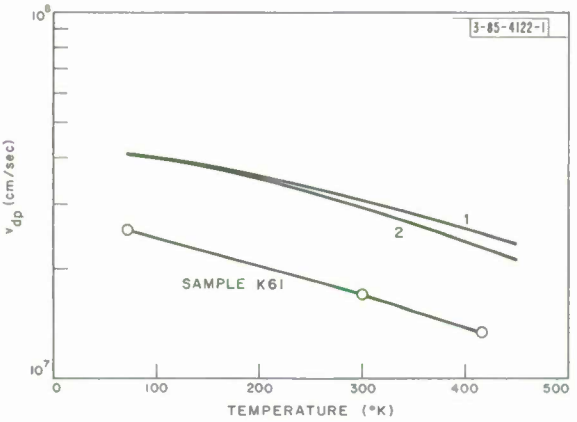

Fig. 22. Threshold electron drift velocity vs temperoture, GaAs.

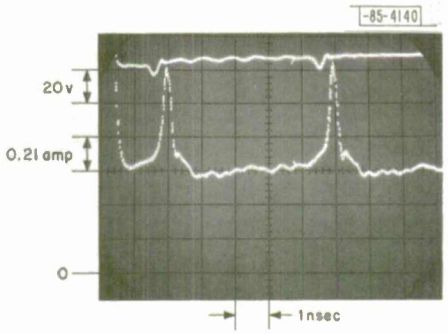

(a) Sample K51, ℓ = 364 microns.

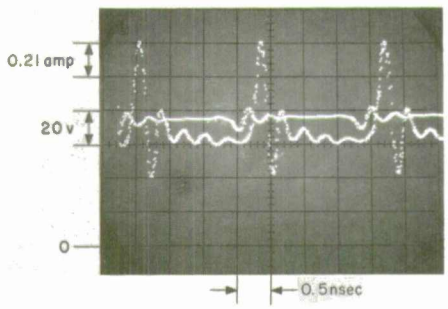

(b) Sample K45, ℓ = 118 microns.

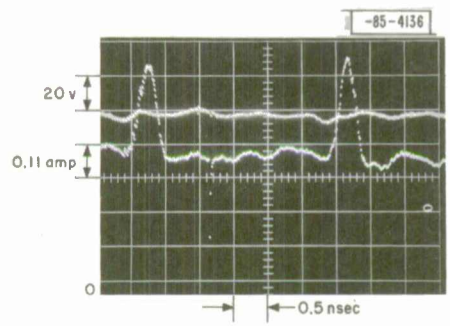

(c) Sample L2(+), ℓ = 272 microns.

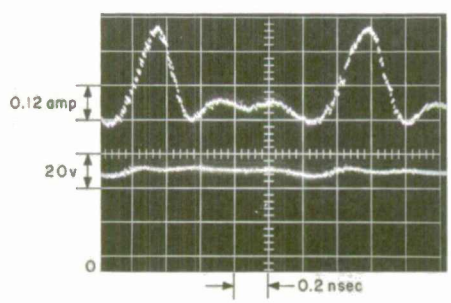

(d) Sample L28, ℓ = 127 microns.

Fig. 23(a-d). Current vs time and voltage vs time, spike waveforms, GaAs, T = 300°K.

TABLE IV

INSTABILITY PERIOD AND ELECTRON TRANSIT TIME FOR LONG SAMPLES

Sample No.	Length (microns)	v_{dv} (units of 10^7 cm/sec)	ℓ/v_{dv} (nsec)	τ (nsec)
K45	118	0.85	1.4	1.75
L28	127	0.98	1.3	1.2
L31	127	1.04	1.22	1.29
M4	145	0.67	2.2	1.6
M5	145	0.9	1.6	1.4
K49	163	0.93	1.8	2.2
L24	200	1.14	1.95	2
L26	200	1.02	2	2.1
K42	272	0.76	3.6	3.5
L2	272	1.01	2.7	3.2
K44	310	0.84	3.7	3.2
K37	326	0.87	3.8	3.5
K51	364	0.71	5.1	5.2
H13	545	1.01	5.45	6.2
L36	763	0.75	10.1	9.8
L34	962	0.79	12.3	11.8

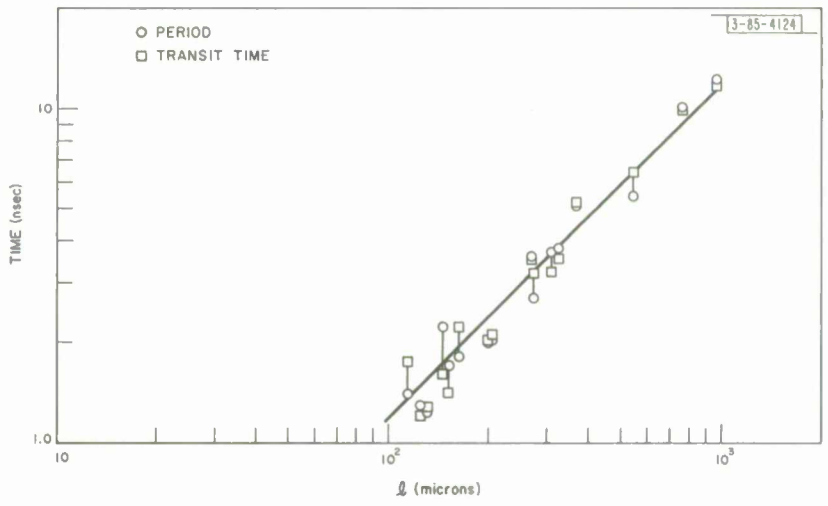

Fig. 24. Instability period and electron transit time vs sample length.

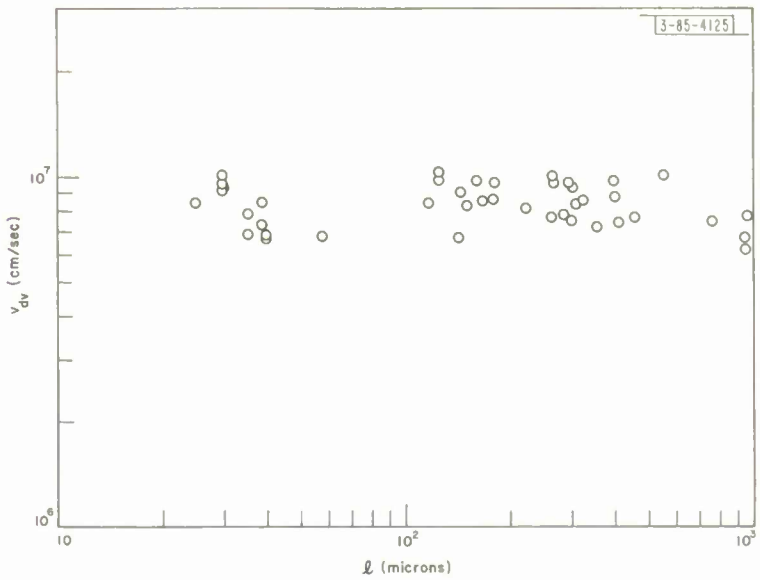

Fig. 25. Volley drift velocity vs sample length, GaAs, T = 300°K.

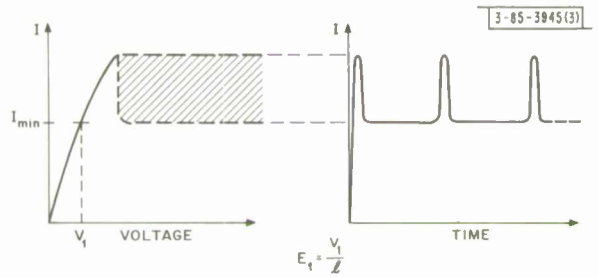

Fig. 26. Evaluation of E_1.

Fig. 27. Domoin voltoge vs sample length, GaAs, T = 300°K.

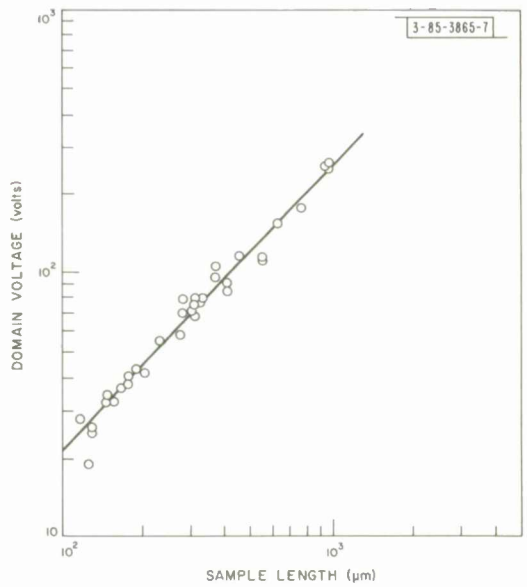

current drops immediately (to within 0.1 nsec, the resolution time of the oscilloscope) and stays at the low value for one period of the instability. The current then rises to the threshold value and the cycle repeats. The peak current for these samples is usually about twice the valley current. The values of the valley drift velocity v_{dv} for all the samples tested are given in Fig. 25 and are plotted vs sample length. We now observe that there is only a slight variation in the average values of threshold electric field and in the peak and valley drift velocities. There is considerable data scatter, and the observed values of these quantities are lower than the predicted values. We also see that our observed threshold electric fields are consistently higher than those observed by Gunn. We were not able to decrease the data scatter. It is known, however, that GaAs of this carrier concentration is not homogeneous and that samples taken from one section of the crystal have different concentrations and mobilities. Furthermore, there are irregularities in the sample, including irregularities in sample cross section and, especially, nonuniformity at the contacts. Such irregularities could cause regions of locally high field and could also cause the instability to start before the average electric field in the sample reached the critical value. In fact, it is suspected that the instability is almost always started by a region of this type, since the sample current vs voltage never reaches saturation.

Another comparison which may be made with the model is the value of E_1 as a function of sample length. For a given sample, E_1 may be evaluated as described below and as illustrated in Fig. 26. As shown, the minimum value of current in the unstable condition is identified as J_{min}. This value of J_{min} is then located on the prebreakdown I-V curve, and a voltage V_1 is determined. Now, in the prebreakdown condition, the electric field is uniform in the sample so that V_1/ℓ should equal E_1, which should be independent of sample length. This was in fact found to be true, and a value of about 1500 volts/cm was found for E_1.

With this information of E_1 and V_1, it was possible to determine the voltage across the high-field domain for each sample. The sample voltage was adjusted to give an average electric field of 4000 volts/cm, and V_1 was subtracted from this applied voltage. From Chap. II, we know that the domain voltage is given by $E_2 x$ = domain voltage = $\bar{E}\ell - E_1\ell$ = applied voltage $- V_1$. We see that for a given average electric field $\bar{E}$, the domain voltage should scale linearly with the sample length and is given by the difference between the applied voltage and $E_1\ell$. This calculated domain voltage vs sample length is shown in Fig. 27, where a linear relation is obtained as expected.*

With the information of domain voltage as a function of sample length, an attempt was made to determine the size of the domain as a function of sample length so that the values of E_2 could be determined. The procedure described in Chap. II was used in which the rise time of current waveform in the spiky mode Δt was attributed to the uniform passage of a high-field domain of width x, moving at the drift velocity of the electrons v_{dv}, so that $x = v_{dv}\Delta t$. Unfortunately, except for the longest samples, this time width was limited by the equipment and was thus not a measure of the domain size. For the longest samples, however, the time width of these spikes increased by a small amount so that it was possible to get an estimate of the domain size. For

*It should be pointed out that Fig. 27 says nothing about how the electric field varies within the domain. In fact, if $n_o \sim 10^{15}/cm^3$, only for samples longer than perhaps 200 microns would we expect the simple Ridley model to hold, since this model neglects the space-charge regions on either side of the domain and assumes the domain field to have a constant value E_2 over a distance x. If the space-charge region on the charge depletion side of the domain is assumed to be fully depleted, we obtain a minimum length of about 4 microns to make the transition from E_2 to E_1 for a sample with $n_o = 10^{15}/cm^3$. The voltage drop across this depletion layer is therefore at least 12 volts, which is about half the entire domain voltage for the 100-micron-long samples.

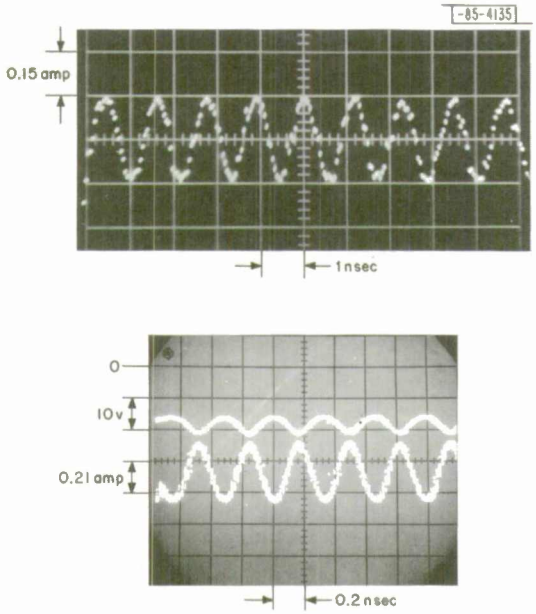

Fig. 28. Current vs time and voltage vs time, sinusoidal woveforms, GaAs, T = 300°K.

TABLE V
INSTABILITY PERIOD AND TRANSIT TIME FOR SHORT SAMPLES

Sample No.	Length (microns)	v_{dp} (units of 10^7 cm/sec)	v_{dv}	ℓ/v_{dp} (nsec)	ℓ/v_{dv} (nsec)	τ_{obs} (nsec)
P20	40	1.3	0.68	0.32	0.59	0.38
N39	38	1.4	0.85	0.28	0.45	0.30
N38	38	1.2	0.74	0.32	0.51	0.30
P16	25	1.7	0.85	0.15	0.3	0.33
P12	40	1.2	0.67	0.33	0.6	0.49
N10	30	1.2	0.94	0.25	0.32	0.30
P10	36	1.2	0.69	0.30	0.52	0.40
P2	30	1.4	0.79	0.21	0.38	0.35
P1	30	1.4	1.01	0.21	0.3	0.31

these samples (sample length ~ 1000 microns), the estimated time of passage of a domain was 40 nsec with a corresponding domain length of 40 microns. By using this number, E_2 was estimated to be 60,000 volts/cm or greater. This value is higher than the 25,000-volt/cm field estimated by Gunn in his probing experiment. However, Gunn stated that his value was a lower bound because of possible circuit limitations. The value of domain voltage measured in Gunn's experiment, 55 volts for a 200-micron sample, does fall on the straight line of Fig. 27 as expected.

2. Sine Waves

The sinusoidal waveform occurs on some of the shorter samples. For samples in the 100-micron length range, this mode may be seen in a narrow range of voltage just above threshold. For these same samples, the waveform goes over into the spike mode as the voltage is increased further above threshold. For shorter samples, a sinusoidal current waveform is seen on the sampling oscilloscope, and it is not clear whether the sinusoidal appearance is due to a frequency limitation of the apparatus or is in fact real. It is known (Chap. III) that the equipment will respond to frequencies of 6 Gcps when the sample is not active, and although there is no simple way to measure the response of the system when the sample is active, as mentioned in Chap. III, it is felt that the response should not be greatly affected. Typical waveforms of this type are shown in Fig. 28.

This type of waveform can be obtained with very little harmonic content. For samples in the 100-micron length range with fundamental frequencies of about 1 Gcps, the harmonic content could be as small as −25 db for the second harmonic and −25 db for the third harmonic. In this situation, no evidence for any other frequencies up to the third harmonic was seen.

The period vs transit time relation is approximately obeyed for these samples, but the transit time is not clearly related to a particular value of velocity as in the previous case. Instead, the period seems to be related to some kind of average velocity, smaller than the peak velocity, but larger than the valley velocity. This average velocity does not seem to bear any simple relation to the peak or valley velocity as shown in Table V, where the values of period are given and compared to the values of transit time computed from the peak drift velocity and the valley drift velocity.

Another complication arises in samples shorter than about 30 microns. For this length range, the period vs transit time relation mentioned above is often followed. However, in many of these samples the frequency is significantly lower than that corresponding to even the valley drift velocity. The amplitude of the instability is usually smaller as the sample length drops below 30 microns, and it has not yet been possible to make a sample shorter than 25 microns with a large instability of the predicted frequency. The origin of this problem is not known, although the variation in results is almost certainly due to contact problems. We know that the requirements on sample preparation and contact alloying become more severe as the sample length is decreased, and it is possible that this difficulty is entirely due to sample preparation techniques. This limitation, however, may be due to a fundamental limit on the instability.

Other types of experiments were performed on samples displaying the sine wave mode. The effects of a DC magnetic field with the sample at room temperature and the effects of external impedance were examined.

A longitudinal DC magnetic field had almost no effect on the amplitude or the frequency of the instability to fields of 15 kG. Above 15 kG the amplitude of the instability decreased with increasing magnetic field, reaching the six-tenths of its zero-field value at 25 kG. A transverse magnetic field, on the other hand, caused a reduction of the instability amplitude at low fields

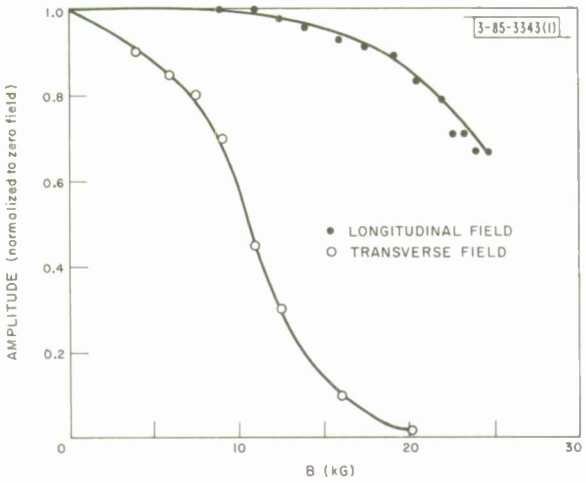

Fig. 29. Instability amplitude vs magnetic field, GaAs, T = 300°K.

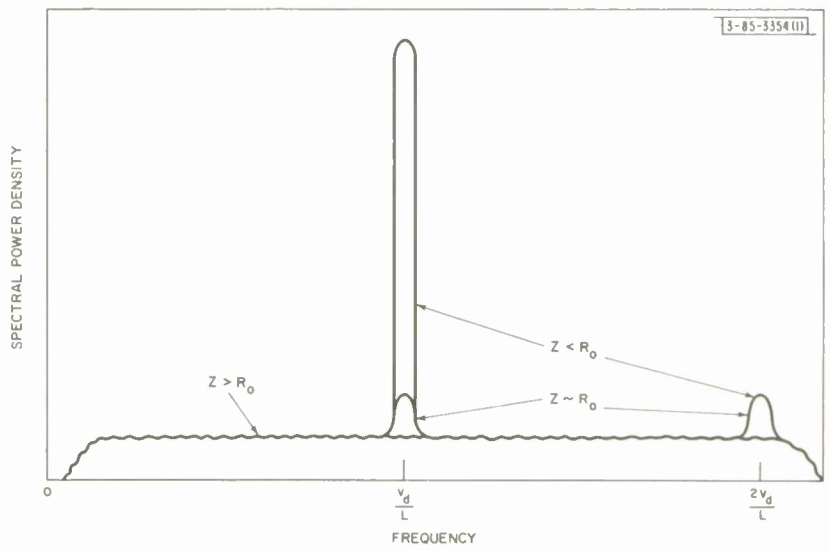

Fig. 30. Spectral power density vs termination impedance, GaAs, T = 300°K.

(about 2 kG) and reduced the instability to less than one-tenth of its low-field value at 20 kG. It is suspected that because of the strong transverse field effect, the effect of the longitudinal field is some kind of residual transverse effect, that is, some misalignment of the field and current or some inhomogeneity in the sample. The amplitude of instability is shown in Fig. 29 for both transverse and longitudinal magnetic fields as a function of the field strength.

The effects of termination impedance were also examined for samples operating in the sine wave mode. It was found that the character of the instability changed as the termination impedance was increased through the sample resistance. As the termination impedance was increased from a value below the sample resistance, the sine wave mode remained essentially unchanged. As the termination impedance was increased through the sample resistance, the sine wave mode disappeared and the instability spectrum, which was narrow in the sine wave mode, became very broadband. The broadband region was not investigated in detail, but it appeared that it was not changed by further increase in termination resistance. For all values of termination impedance, the prebreakdown current vs voltage curve and the instability threshold were unchanged. A pictorial sketch of the instability output vs frequency for several values of termination impedance is shown in Fig. 30 and the instability bandwidth vs termination impedance is shown in Fig. 31.

3. Other Waveforms

In other samples, neither the spike nor the sine waveforms are seen. Instead, a variety of waveforms are seen, which may be grouped into two further classes: first, waveforms which are large in amplitude and which are repetitive, but which are not seen on any other sample; and second, small amplitude instabilities, which are initiated by low values of threshold electric field (about 1500 to 2000 volts/cm for 200-micron samples). Some examples of the first type of waveform are shown in Fig. 32. The threshold fields and velocities for these samples are usually similar to the values for the spike waveforms. However, the period vs transit time relation is not usually obeyed. Instead, the measured period is shorter than the transit time $\tau = L/v_{dv}$ – often several times shorter, with no obvious harmonic relation to the fundamental period. This class of waveforms resembles the waveforms obtained by Gunn in his original investigations. This observation of the similarity of waveforms leads us to a speculation on the cause of such waveforms. Gunn's method of sample fabrication differed from ours in the way in which the sample surfaces were prepared and the way in which contact was made. We know from other tests that since the condition of the side surfaces of a sample does not have an appreciable effect on the instability, we are left with the difference in method of contacting. It is suspected from the relative reproducibility of our results that our method of contacting yields contacts that are more uniform. We therefore suspect that the cause of the unusual waveforms is in the contacts, probably because of nonuniform alloying, and thus not characteristic of the effect.

The last class of waveforms that has been seen in this study can be characterized as small amplitude instabilities. These instabilities usually occur at low threshold electric fields and exhibit an instability that is small in amplitude and that is not coherent on the sampling oscilloscope. This class of waveforms was first seen in an experiment that was performed on GaAs to ascertain if the Gunn effect were present only with a tin contact or if other ohmic contact materials could be used. The only other material used which gave an ohmic contact to n-type GaAs was indium-doped with tellurium. This type of contact had to be alloyed rapidly to prevent loss of the tellurium by evaporation. Consequently, the alloying operation was done as

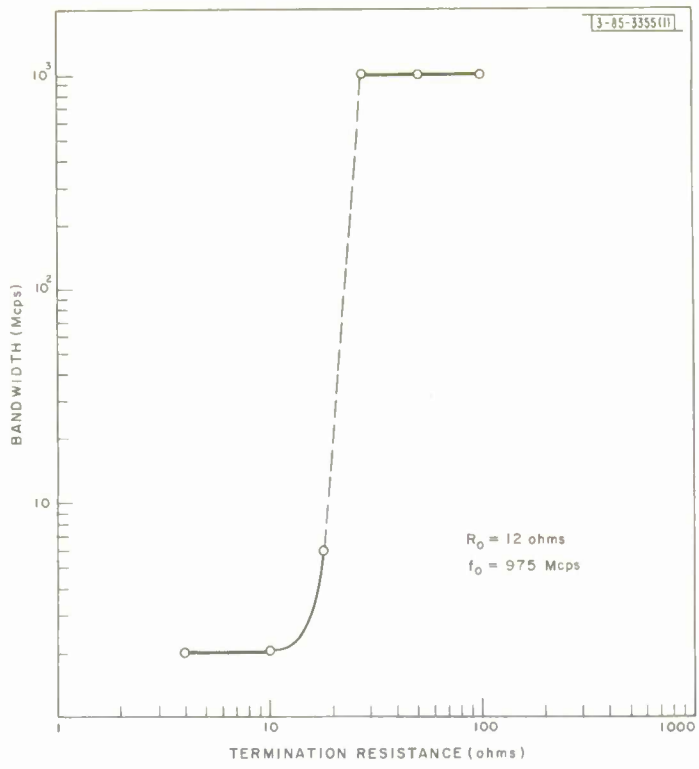

Fig. 31. Instability bandwidth vs terminotian impedance, GaAs, T = 300°K.

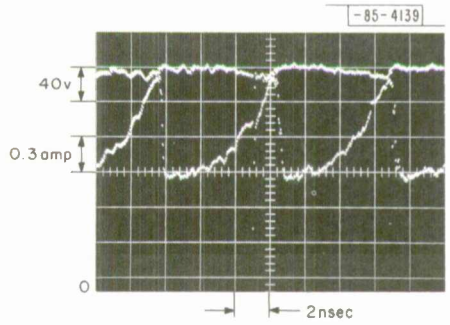

(a) Sample H9, ℓ = 635 microns.

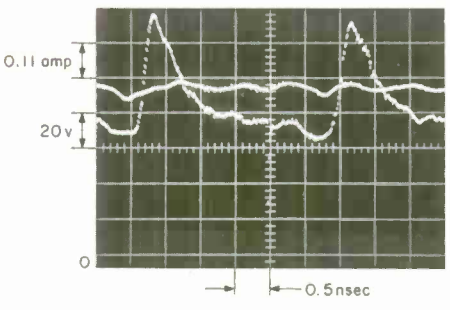

(b) Sample L2(-), ℓ = 272 microns.

Fig. 32(a-b). Current vs time and voltoge vs time, anomalous woveforms, GaAs, T = 300°K.

rapidly as possible – a fraction of a second. Samples prepared in this way were ohmic with about the correct value of low-field resistance.

The instability did occur in most of these samples. However, it occurred at low values of threshold electric field around 1500 volts/cm and was characterized by a small, incoherent instability. A question naturally arose as to why the instability should be present but small. To resolve this question, a similar fast alloy procedure was used for alloying tin onto some samples; it was found that the instability occurred in these samples at low values of threshold electric field and was characterized by a small amplitude incoherent waveform just as for the In-Te contact samples. This experiment was not pursued further since the results were somewhat erratic and uninteresting. However, it seemed that once again the problem could be explained by poor contacts because of the rapid alloying procedure.

B. CdTe

We examined CdTe for the Gunn effect with a positive result. The sample was n-type CdTe grown and evaluated by the General Electric Research Laboratory, Schenectady.[34] It had a room temperature carrier concentration of 5×10^{14}/cc and a mobility which was determined only by polar optical mode scattering from room temperature to 77°K. The room temperature mobility was 1100 cm^2/volt-sec, which increased to 57,000 cm^2/volt-sec at 77°K. The (scalar) effective mass for the lowest (zone centered) minimum was 0.11 m_e.

Samples of this material were examined for current instabilities as described in Chap. III. A voltage vs current curve for one sample at room temperature is shown in Fig. 33 and the corresponding current vs time and voltage vs time waveforms, in the unstable condition, are shown in Fig. 34. In order to compare this result with the model of Chap. II, we must determine the location of the higher conduction band minima, and hopefully, the effective mass in the higher minimum. Since this information did not seem to be known, a study was initiated to determine

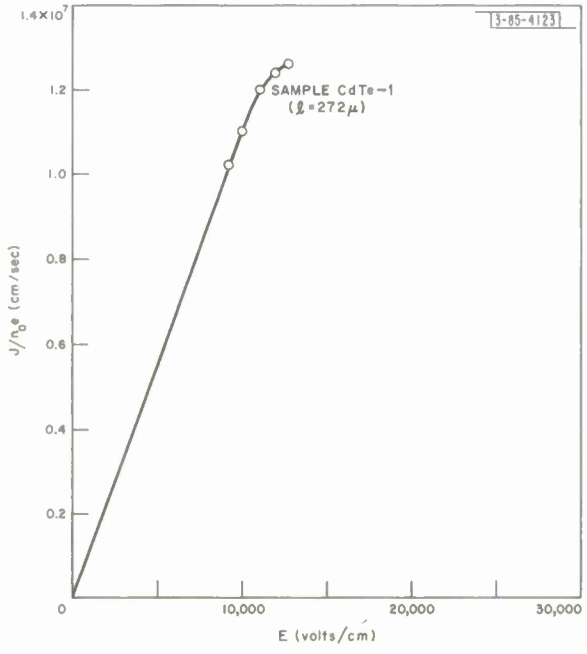

Fig. 33. Sample current vs voltage, CdTe, T = 300°K.

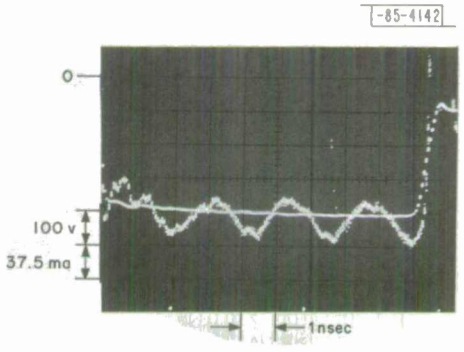

Fig. 34. Current vs time and voltage vs time, CdTe, T = 300°K.

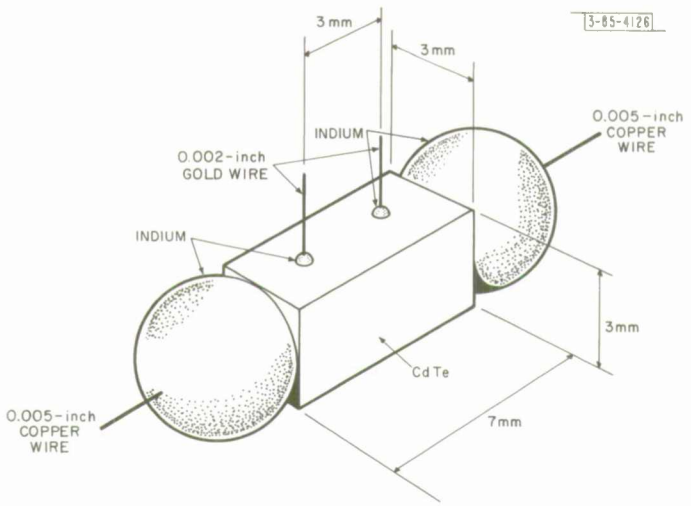

Fig. 35. Sketch of sample used for CdTe resistance vs hydrostatic pressure.

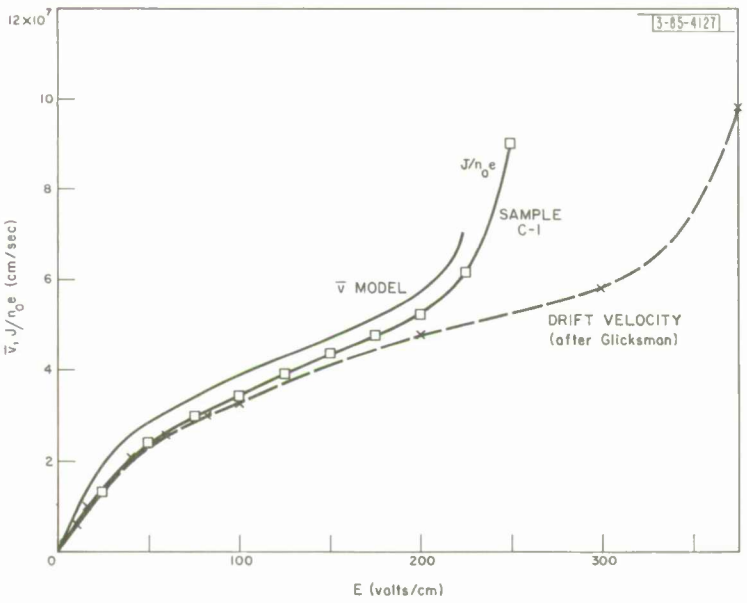

Fig. 36. Sample current vs voltage, InSb, T = 77°K.

the location and mass of the higher minima. The experiment that appeared most promising was an experiment of the effects of hydrostatic pressure on the resistance of this material at room temperature. Such an experiment had already been done on n-type GaAs by Howard and Paul[32] to demonstrate the existence of higher minima in that material. Our experiment in collaboration with Professor W. Paul of Harvard University proceeded as follows. A bar of the same material that was used to make the oscillator samples was fashioned into a four-point resistance sample by alloying four indium contacts onto the sample. The resulting sample is shown in Fig. 35. This sample was placed in the hydrostatic pressure apparatus used by Howard and Paul, and the resistance was measured as a function of pressure at room temperature. The resistance did increase with pressure in a manner consistent with the transfer of electrons into a lower mobility minimum. The preliminary data indicate the presence of a set of minima located a few tenths of an electron volt above the lowest minimum.

C. InSb

InSb was examined for current instability at 77°K with a negative result. The voltage vs current curves for InSb did not show a saturation at high fields as did the samples of GaAs and CdTe. Instead, the current began to increase rapidly as the electric field approached about 250 volts/cm. The measured current vs voltage curve is shown in Fig. 36. A comparison with the model of Chap. II is difficult, however, because it is known that carrier multiplication occurs for fields exceeding about 200 volts/cm[10]. For fields below 200 volts/cm, however, the carrier concentration is constant, and the current is linearly related to the electron velocity. For these fields, the comparison of experimental drift velocity (also the experimental results of Glicksman and Hicinbothem[10]) with the calculated drift velocity is in good agreement. Above this value, carrier multiplication obscures the current vs drift velocity relation, and a comparison with the model is not possible. However, the experimental results of Glicksman and Hicinbothem, which included both Hall effect and conductivity measurements, yielded the drift velocity vs electric field curve shown in Fig. 36.

Theoretically, the prediction of drift velocty vs electric field curve is complicated by the highly nonparabolic conduction band in InSb. This complication causes the apparent effective mass of the electrons to increase as the energy of the electrons increases so that it becomes more difficult to increase the carrier velocity with electric field. Glicksman takes this effect into account in calculating drift velocity vs electric field curves, whereas the model of Chap. II does not. However, even with these corrections, Glicksman is not able to achieve a quantitative agreement with experiment in the high-field region. A possible source of this difficulty is the choice of values for ϵ_s and ϵ_∞. Glicksman chooses $\epsilon_s = 18.7$ and $\epsilon_\infty = 15.7$ so that $\epsilon_s - \epsilon_\infty = 3$. A more recent paper[36] gives $\epsilon_s - \epsilon_\infty = 2$ for InSb, which would bring the high-field prediction of Glicksman and Hicinbothem into better agreement with the experimental results.

In any case, the effect of carrier multiplication would further prevent the occurrence of a negative resistance in this material.

D. InAs

InAs was examined for a current instability with negative results, both at room temperature and at 77°K. Instead, the current began to increase rapidly for electric fields ~ 1100 volts/cm.

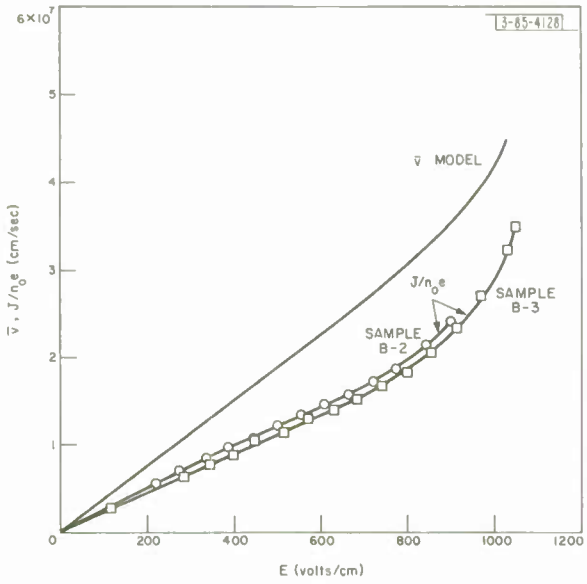

Fig. 37. Sample current vs voltage, InAs, T = 300°K.

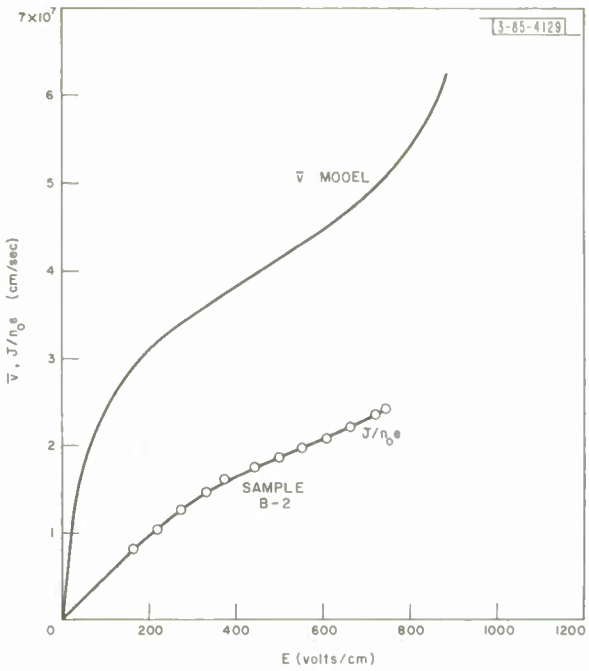

Fig. 38. Sample current vs voltage, InAs, T = 77°K.

The experimental current vs electric field curves are shown in Figs. 37 and 38, with the predicted velocity vs electric field curves of Chap. II shown for comparison. This material is, as is InSb, a low energy gap semiconductor, and the possible complications due to carrier multiplication and a nonparabolic conduction band may be important. Since these effects apparently have not been studied in InAs, it is not possible at this time to separate the effects of velocity increase from those of carrier multiplication. In addition, there are other scattering mechanisms which limit the low-field mobility to values lower than those predicted for polar optical mode scattering alone.

In spite of these complications, the experimental results at room temperature are in reasonable agreement with the model, especially the value of critical electric field.

CHAPTER V
DISCUSSION AND CONCLUSIONS

The experimental results presented in Chap. lV are generally in qualitative agreement with the model of Chap. ll. lf an instability is predicted for a given material, an instability is seen experimentally. There are, however, quantitative differences between the model and each of the materials studied. These will be examined separately for each material.

A. GaAs

The spike mode seen in GaAs is in qualitative agreement with the model of Chap. ll. ln order to make a quantitative comparison, the important parameters are summarized in Table Vl, where the experimental values are compared to the predicted values for the two cases discussed in Chap. ll.

TABLE VI
COMPARISON OF MODEL AND EXPERIMENT FOR GaAs

Parameter	Experimental Value	Predicted Values	
		Case 1	Case 2
E_p	2,300 – 4,000 volts/cm	6,700	7,900
E_1	1,400 – 1,700 volts/cm	4,300	1,800
E_2	60,000 volts/cm	12,000	48,000
V_{dp}	$1.1 - 1.65 \times 10^7$ cm/sec	3×10^7	2.9×10^7
V_{dv}	$0.67 - 1.0 \times 10^7$ cm/sec	2.7×10^7	1.47×10^7

We see that, in order to achieve a reasonable quantitative agreement with the experimental results, it is necessary to attribute all the mobility ratio between the two sets of minima to an increase in the mass, which is probably an unreasonable assumption in view of the work of Ehrenreich. The most likely reason for the lack of quantitative agreement is that the model is too simplified, and the assumption of a common electron temperature is not accurate.

Another discrepancy between the experiment and the model is that the experimental current never reaches a saturation before an instability begins. This discrepancy was attributed in Chap. IV to regions of locally high field which started an instability before the rest of the sample reached that field. An interesting confirmation of this interpretation lies in the observation of small amplitude instabilities which occurred in the rapidly alloyed samples. For these cases, an instability was seen for electric fields greater than about 1500 volts/cm, but the instabilities

were of small amplitude and were not coherent as seen on the sampling oscilloscope. This result may be interpreted in the following way: The region of alloy-semiconductor contact is a region of locally high electric field strength and may generate a high-field domain at low values of average electric field; however, this domain will not propagate along the sample unless the average electric field in the sample is greater than E_1, the minimum value for which the domain configuration will be stable. Thus, although a high-field domain might be generated at a contact, it will not propagate and thus will not be seen in the external circuit unless the average electric field in the sample exceeds E_1, about 1500 volts/cm. For fields in excess of this value, the domain will propagate. But, since the fields required for generation and for propagation are nearly the same, the resulting instability will be small. It is felt that the variation in threshold electric fields which has been observed by many workers in this field is due to contact problems of this sort and to inhomogeneities in material.

The effects of temperature variation are also in qualitative agreement with this model. The values of threshold electric field and of peak electron drift velocity exhibit the same dependence on temperature as is predicted by the model. As noted in Chap. IV, however, the predicted values of electric field are considerably higher than the observed values.

The sinusoidal mode is not predicted by the simplest form of the transferred electron model. It has been suggested by Kroemer[23] that this mode is a charge accumulation type (compared to the dipole type of the spike waveforms) and by Gunn that this mode is an incipient form of the spike mode, both resulting from the same negative resistance curve. One possible clue to this change from spike to sine wave mode is to look at the width of the space-charge region necessary to make the transition from E_2 to E_1. If we assume that the space-charge region on the charge depletion side is completely depleted, we can obtain a minimum value for the size of this transition region. For the samples of smallest carrier concentration ($n \approx 2 \times 10^{14}$/cc), this estimate gives a minimum size of 20 microns. Thus, for samples in the 100-micron length range, this transition region is larger than the high-field domain (length ~ 3 microns) and is the same order as the sample size. It appears likely that the change in the character of the instability could be caused by the size of this region becoming comparable to or larger than the high-field region, although this conjecture has not been examined in detail. The other experiments performed on samples operating in this mode, those of magnetic field dependence and of dependence on external impedance, are consistent with the interpretation of the instability as a longitudinal disturbance caused by a negative resistance.

B. CdTe

Although CdTe did exhibit an instability similar to that seen in GaAs, the instability did not have a large amplitude, nor did it have the spike-like waveform that was characteristic of GaAs samples of the same length. The most likely cause for this difficulty is poor contacts – as in the case of the GaAs samples that exhibited anomalous behavior. The only type of alloyed contact which was found to be ohmic to CdTe was indium alloyed rapidly (liquid for less than one second). As noted in the GaAs experiments, this procedure led to instabilities which were smaller in amplitude than when a slow alloy was used. However, attempts to use a slow alloy for indium and CdTe were not successful; samples alloyed slowly were usually non-ohmic and, quite often, of very high resistance. It is surprising, in fact, that the instability observed in this case was sufficiently large to be observed, because none of the fast alloy GaAs samples

displayed an instability that was observable as a repetitive waveform. This observation suggests that CdTe might be capable of a larger peak-to-valley-current ratio if the contact problem could be solved.

C. GENERAL COMMENTS AND CONCLUSION

The materials examined in this study may be divided into two classes: those which show a tendency toward current saturation with increasing voltage, and which exhibit an instability; and those which show a tendency toward current runaway with increasing voltage, and which do not exhibit an instability. In order to interpret these results, let us for the moment ignore the subsidiary conduction band minima and consider only the lowest minimum. For this single band, the theory of polar optical mode scattering predicts a critical electric field, above which the electrons lose their ability to interact with the lattice and experience a large increase in energy. Using Stratton's model,[12] this critical field has been calculated for InP as well as for GaAs and CdTe. The values are given in Table VII and compared with the observed threshold electric field for the Gunn effect.

TABLE VII

COMPARISON OF PREDICTED CRITICAL ELECTRIC FIELD AND OBSERVED THRESHOLD FIELD

Materiol	Temperature (°K)	Energy Gap (ev)	Energy Separatian af Conductian Band Minima (ev)	Gunn Effect	Predicted Criticol Field (valts/cm)	Threshald Field (valts/cm)
GaAs	300	1.35	0.36*	Yes	3,600	2,500 – 4,000
InP	300	1.25	0.4†	Yes	7,800	7,200‡
CdTe	300	1.5	unknawn	Yes	12,900	13,000
InAs	300	0.36	1.1§	Na	–	–
InSb	77	0.22	0.6§	No	–	–

*Ref. 16.

†Ref. 38 (deduced by Edwords ond Drickomer from the shift of opticol absarptian edge with pressure).

‡Ref. 1.

§Ref. 35 (extropolotions by Hilsum of energy gaps from ather III-V semiconductors ond from mixed crystols).

Two things are apparent from this table. First, there is close agreement between the predicted critical field and the threshold field at which Gunn oscillations occur.* Second, an instability is present only in those materials for which the energy gap between the valence band and lowest conduction band is larger than the separation between the conduction band minima. It thus appears that an instability will occur only if the electrons can populate low-mobility subsidiary conduction band minima before they acquire enough energy to cause impact ionization across the gap. If the carriers acquire enough energy to impact ionize hole-electron pairs first, then the current density will increase rapidly and no negative resistance will be obtained.

*Of course, if the energy separation between the conduction band minimo is very small, a situation achieved in the GaAs pressure experiments,[27] then the threshold field con be considerably less thon the runaway field.

APPENDIX A
CALCULATION OF EFFECTIVE MASS FROM MOBILITY RATIOS

In order to calculate the effective mass in the higher conduction band minima in GaAs from the experimental ratio of mobilities between the lowest minimum and these higher minima, we have assumed that the mobility in each minimum is determined by polar optical mode scattering and that the anisotropy in the higher minima is the same as for silicon. With these assumptions, and following Ehrenreich's analysis, the mobilities in the lowest and highest valleys are given by

$$\mu_1 = \frac{e\tau_1}{m_1} \sim \frac{1}{(m_1)^{3/2}}$$

$$\mu_2 = \frac{e\tau_2}{m_{c2}} \sim \frac{1}{m_{c2}(m_{\rho 2})^{1/2}}$$

where m_1 is the mass of the lowest (spherical) minimum, and m_{c2} and $m_{\rho 2}$ are the conductivity and density of states effective masses, respectively, for each of the higher valleys. The expressions relating m_{c2} and $m_{\rho 2}$ to the longitudinal mass m_ℓ and the transverse mass m_t of the higher valleys are given[39] by

$$m_{c2} = \frac{3K}{2K+1}\, m_t$$

$$m_{\rho 2} = (K)^{1/3}\, m_t$$

where $K = m_\ell/m_t$.

With these expressions, the mobility ratio may be written in terms of a mass ratio, as

$$\frac{\mu_1}{\mu_2} = \frac{m_{c2}(m_{\rho 2})^{1/2}}{(m_1)^{3/2}} = \left(\frac{m_t}{m_1}\right)^{3/2} \frac{3K}{2K+1}\,(K)^{1/6}$$

or

$$(1.8)\left(\frac{m_t}{m_1}\right)^{3/2} = \frac{\mu_1}{\mu_2}$$

for K = 5.1. If we now use the estimate of 55 for mobility ratio, we obtain $m_t = 9.2\, m_1 = 0.66\, m_e$, for $m_1 = 0.072\, m_e$, which gives the following values for $m_{\rho 2}$ and m_{c2}:

$$m_{\rho 2} = 1.2\, m_e$$

$$m_{c2} = 0.96\, m_e \quad .$$

These values are for one minimum, and the total density of states in the higher minima would be six times the density of states for one minimum. If we modify the density of states mass to account for this multiplicity, we obtain

$$m'_{\rho 2} = (6)^{2/3}\, m_{\rho 2} \approx 3.98\, m_e$$

which is the value used in Chap. II.

APPENDIX B
DETAILS OF SAMPLE PREPARATION

This appendix contains the details of sample preparation which were omitted from the main text. Although the several materials used in this study were prepared in a similar manner, there were significant differences in the preparation, especially in the alloy process, that affected the performance of the samples. The following steps summarize the procedure:

(1) A slice of the material was cut from an ingot, in the desired orientation, with an abrasive saw.

(2) The slice was mounted on a stainless steel polishing cylinder with wax, and the exposed surface was polished with standard carborundum paper and water-abrasive solutions. It was then demounted from the polishing block and remounted with the opposite face exposed. This face was polished in a similar manner until the slice thickness was about 0.0005 inch greater than the desired thickness. The slice was again demounted from the polishing block.

(3) The slice was cleaned to remove wax, grease, and other surface dirt by successive immersion in boiling water and alconox, clean water, boiling isopropyl alcohol, boiling acetone, boiling isopropyl alcohol again, and boiling acetone again.

(4) The slice was etched in a ten-percent (by volume) solution of bromine in methyl alcohol for about fifteen seconds at room temperature. This etch was followed by three rinses in methyl alcohol after which the slice was dried and placed on filter paper in a small container.

(5) The slice was then cleaved into smaller pieces by using a microscope slide and a pair of fine tweezers.

(6) The resulting sample was placed on a carbon heater strip in a hydrogen atmosphere with a small sphere of contact material resting on opposite ends of the sample. A small amount of $AlCl_3$ was placed at the ends of the heater strip to provide HCl vapor when the alloying took place. Current was passed through the heater strip so that the sample and contact material were heated to the alloying temperature. This step contains the only basic difference in the processing of the various materials and will be discussed for each of the materials.

> GaAs: Two types of contact material were used for GaAs: pure tin, and indium doped with one-percent tellurium. The tin contacts were alloyed at temperatures ranging from 320° to 400°C, with the alloying temperature maintained for about five to ten seconds (a slow alloy). The In-Te contacts, on the other hand, had to be alloyed rapidly to prevent loss of the tellurium. This was done by applying full power to the heater strip, so that its temperature increased rapidly, and then turning off the power as the strip temperature approached the desired alloy temperature. The highest temperature reached for the In-Te was about 400°C, and the time that the alloy was melted was on the order of one second. Both these contacts were ohmic and both gave the instability. However, as noted in the main text, the In-Te contacts gave only small amplitude instabilities.
>
> CdTe: Indium was a satisfactory contact for this material, but it had to be alloyed rapidly. A procedure similar to that for GaAs was used, except that the highest temperature was about 300°C.
>
> InSb and InAs: Tin was a satisfactory contact for these materials, and a slow alloy procedure was used. The temperature of alloying was about 250°C in both cases.

(7) After the alloying operation, the low-field resistance of the sample was measured. If this resistance was consistent with the bulk properties of the material, the sample was mounted in a standard tunnel diode package by the following procedure. A small amount of low-melting-point solder (cerroseal 35) was melted onto the copper pedestal of the package which was then cooled to room temperature. A drop of liquid flux was placed on the solder, and one end of the sample floated in the flux. The package was reheated to alloy the solder to the contact material on the end of the sample. A small (0.002- to 0.005-inch diameter) wire was soldered between the flange on the package and the top end of the sample to complete the preparation. The sample was then cleaned in a water solution of alconox, followed by immersion in clean water, alcohol, and finally acetone to remove the residue of the soldering operation. The sample was ready for electrical evaluation at this point.

ACKNOWLEDGMENT

The author expresses his appreciation to Professor A. L. McWhorter for his guidance, encouragement, and criticism throughout the present work. He also wishes to thank Professors R. B. Adler and A. Bers for several discussions regarding possible mechanisms for the Gunn effect.

Further thanks go to Dr. R. E. Halsted of the General Electric Research Laboratory for the samples of CdTe; to Professor W. Paul of Harvard University for making the pressure experiments on CdTe possible; and to Mrs. Nancy Rowson for performing the computer calculations.

Finally, the support of Lincoln Laboratory, Division 8 and Group 85 in particular, is gratefully acknowledged.

REFERENCES

1. J. B. Gunn, Solid-State Device Research Conf., 12-14 June 1963.
2. J. B. Gunn, Solid State Commun. 1, 88 (1963).
3. J. B. Gunn, IBM J. Research Develop. 8, 141 (1964).
4. E. J. Ryder, Phys. Rev. 90, 766 (1953).
5. E. J. Ryder and W. Shockley, Phys. Rev. 81, 139 (1951).
6. J. B. Arthur, A. F. Gibson, and J. W. Granville, J. Electronics 2, 145 (1956).
7. J. B. Gunn, J. Electronics 2, 87 (1956).
8. W. Shockley, Bell System Tech. J. 30, 990 (1951).
9. E. Conwell, J. Phys. Chem. Solids 8, 234 (1958).
10. M. Glicksman and W. A. Hicinbothem, Jr., Phys. Rev. 129, 1572 (1963).
11. J. Bok, C. Guthmann, Physico Stotus Solidi 6, 853 (1964).
12. R. Stratton, Proc. Roy. Soc. (London) A246, 406 (1958).
13. H. Frohlich, Proc. Roy. Soc. (London) A160, 280 (1937).
14. B. V. Paranjape, 1953 Rep. Brit. Elect. Ind. Res. Ass. L/T 285; Proc. Phys. Soc. B70, 628 (1956).
15. H. Frohlich and B.V. Poranjape, Proc. Phys. Soc. B69, 21 (1956).
16. H. Ehrenreich, Phys. Rev. 120, 1951 (1960).
17. D. J. Howarth and E. H. Sondheimer, Proc. Roy. Soc. (London) A219, 53 (1953).
18. J. M. Ziman, Electrons and Phonons (Oxford University Press, London, 1960).
19. J. B. Gunn, Symp. Plasma Effects in Solids, Paris, 1964; also Am. Phys. Soc., Kansas City, Missouri, March 1965.
20. B. W. Hakki and J. C. Irvin, Proc. IEEE 53, 80 (1965).

21. T.M. Quist ond A. G. Foyt, Proc. IEEE 53, 303 (1965), DDC 622309.

22. N. Broslou, J.B. Gunn, ond J. L. Stoples, IBM J. Reseorch Develop. 8, 545 (1964).

23. H. Kroemer, Proc. IEEE 52, 1736 (1964).

24. C. Hilsum, Proc. IRE 50, 185 (1962).

25. B. K. Ridley, Proc. Phys. Soc. (London) 82, 954 (1963).

26. G.F. Doy, Am. Phys. Soc., Konsos City, Missouri, Morch 1965.

27. A.R. Hutson, A. Jayoromon, A. G. Chynoweth, A.S. Coriell, ond W.L. Feldmon, Phys. Rev. Letters 14, 639 (1965).

28. B. K. Ridley ond T. B. Wotkins, Proc. Phys. Soc. (London) 78, 293 (1961).

29. Tobles of the Bessel Functions, NBS Applied Mothemotics Series 25 (U. S. Government Printing Office, Woshington, 1952).

30. G. N. Wotson, Theory of Bessel Functions (Combridge University Press, London, 1958).

31. C. Hilsum ond A. C. Rose-Innes, Semiconducting III-V Compounds (Pergomon Press, London 1961).

32. W. Howord ond W. Poul, os shown in H. Ehrenreich, Phys. Rev. 120, 1951 (1960).

33. A. R. Hutson, A. Joyoromon, ond J. H. McFee, Am. Phys. Soc., Chicogo, Illinois, October 1964.

34. N. Segoll, M. R. Lorenz, ond R. E. Holsted, Phys. Rev. 129, 2471 (1963).

35. C. Hilsum, Proc. 7th Internot. Conf. Physics of Semiconductors, Poris, 1964, p. 1127.

36. M. Hoss ond B. W. Henvis, J. Phys. Chem. Solids 23, 1099 (1962).

37. H. Kroemer, Interim Engineering Report No. 6, Air Force Systems Commond, Wright-Potterson Air Force Bose (April 1965).

38. A. L. Edwords ond H. G. Drickomer, Phys. Rev. 122, 1149 (1961).

39. R. A. Smith, Semiconductors (Combridge University Press, 1959).

DOCUMENT CONTROL DATA – R&D

(Security classification of title, body of abstract and indexing annotation must be entered when the overall report is classified)

1. ORIGINATING ACTIVITY *(Corporate author)* Lincoln Laboratory, M. I. T.	2a. REPORT SECURITY CLASSIFICATION Unclassified 2b. GROUP None

3. REPORT TITLE

Gunn Effect in Compound Semiconductors

4. DESCRIPTIVE NOTES *(Type of report and inclusive dates)*

Technical Report

5. AUTHOR(S) *(Last name, first name, initial)*

Foyt, Arthur G., Jr.

6. REPORT DATE	7a. TOTAL NO. OF PAGES	7b. NO. OF REFS
7 July 1965	56	39

8a. CONTRACT OR GRANT NO. AF 19(628)-5167 b. PROJECT NO. 649L c. d.	9a. ORIGINATOR'S REPORT NUMBER(S) Technical Report 385 9b. OTHER REPORT NO(S) *(Any other numbers that may be assigned this report)* ESD-TDR-65-306

10. AVAILABILITY/LIMITATION NOTICES

Distribution of this document is unlimited.

11. SUPPLEMENTARY NOTES	12. SPONSORING MILITARY ACTIVITY
None	Air Force Systems Command, USAF

13. ABSTRACT

A theoretical and experimental study of the Gunn effect is presented. It appears that this effect, originally observed by Gunn as a time variation in the current through ohmic samples of n-GaAs when the sample voltage exceeded a critical value, can be accounted for by the transferred electron model of Ridley and Watkins. This model is based on a transfer of electrons from a low-mass, high-mobility conduction band that is lowest in energy to a higher-mass, low-mobility band as the electron temperature is increased by the applied electric field. If the transfer occurs rapidly enough as the electric field is increased, a bulk differential negative resistance will be realized, which then leads to the formation of domains of different electrical conductivity which move through the sample, giving rise to a time-varying current.

The Gunn effect has also been observed in n-CdTe, and resistance vs hydrostatic pressure experiments show that the transferred electron model is a reasonable explanation for this material as well.

Finally, the absence of an instability in n-InSb and n-InAs is shown to be consistent with the transferred electron model. The higher conduction band minima in these materials are probably sufficiently separated from the lowest minimum that other effects, such as carrier multiplication, will occur before transfer, and no negative resistance is to be expected.

14. KEY WORDS

Gunn effect
semiconductors
high electric field effects
hot electrons
gallium arsenide
cadmium telluride
indium antimonide
indium arsenide